Answers to the reviewers

We would like to thanks the reviewers for the useful comments and insights that allowed us to better redefine the methods and presenting the results of this study.

First reviewer:

General comments

5   *" [. . .]in the analysis of the effect of RH on the aerosol linear depolarization ratio (δ_a) , a correlation analysis between the RH at surface level and the values of δ_a at the lowest altitudes would offer more information about this process"*

Following the suggestions of the rewiever, we adopted a more quantitative approach to describe the near ground hygroscopic growth events. A correlation analysis between the ground RH and the δ_a along the time would not be meaningful, as the

10   variability of aerosol depolarization near the ground is not affected solely by RH. We decided instead to better show, along the whole campaign period, the effect of different values of RH along the vertical profile of δ_a for dust and dust-free days. Details can be find in the answer to point "10. Issues regarding section 7"

     " According to the authors, "The main objective of this paper is to investigate the transport of desert dust in the middle troposphere and its intrusion into the planetary boundary layer (page 1, line 4)". In order to fulfil this objective it would be

15   *desirable a more detailed analysis of the events where the aerosol concentration increases at surface level and how the dust layer interacts with the PBL. However, the whole 21-day period is presented in a single figure (figure 2, lidar; figure 4, in situ). "*

To facilitate the individuation of dust intrusion in the PBL and its penetration down to the ground, a closer view is added (see Fig 5 of the revised manuscript). Here we show LiDAR aerosol particle types profiles, and the corresponding APSS volume

20   size distribution of aerosol particles at the ground, during the dust events. The interaction of dust with the PBL and the direct effect of the dust layer intrusion on the particles concentration at the ground it's thus more easily identifiable.

     " A great part of this work is based on measurements of a lidar system. However, the lidar signals have not been properly processed. The calculations regarding the lidar measurements must be revised (see specific comments). "

Reviewer comments highlighted the need to revise the section on the adopted LiDAR signal processing. We rewrote this

25   section to remove any ambiguities in the parameters definition. See also answers to points 2, 4 and 5.

     " Finally, the authors must carry on a thorough revision of the language. "

We revised the manuscript to improve the language.

Specific comments

" *1. Page 4, line 20: "In the following discussion, we will make use of backscattering ratio (R)". Why do the authors use R, which depends on the molecular terms, rather than β_a, which only depend on aerosols?* "

5

The use of the total backscattering ratio R instead of the aerosol backscatter β_a, has the advantage to be bereft of the noise that is introduced by the signal inversion for β_a estimation. This helps to have a refined aerosol classification. In the paper we therefore based the aerosol classification on the parameter 1-1/R, varying from 0 to 1 accordingly to the presence of an aerosol layer, instead of relying directly on R values. To emphasize the meaning of such parameter we changed its expression as a

10 function of the aerosol backscattering ratio (Ra=R-1= β_a(r)/ β_m(r)) instead of R. Classification is now a function of the values of Ra/(Ra+1), still varying from 0, when β_a(r)=0, to 1, when in presence of dense aerosol layer (high β_a(r) values).

" *2. [. . .] I could not get to understand how the authors use δ_a to determine the lidar ratio prior to the signal inversion. However, in page 4, line 29 the authors claim: ". . . desert dust (identified by δ_a (r) > 10%) is characterized by L equal to 50*

15 *sr (Müller et al., 2007). . . ". This is the same criterion used by Rosety [2016], although Rosety [2016] used δ instead of δ_a. Because of this, the most likely explanation is that the authors have mixed up both parameters (δ and δ_a). Another example of this is found in page 6, line 29 [. . .] Nevertheless, the authors barely find aerosols with δ_a > 20 % (e.g., Fig. 1). This is another indication that the authors are actually using δ instead of δ_a. Page 7, line 3: [. . .] Again, I think that these differences are because the authors are comparting two different parameters (δ and δ_a). The authors should revise their calculations to see if*

20 *this is the source of disagreement. If, after this, the calibration stills play an important role in this disagreement, the authors should describe its effect in a more detailed way. In the corrected version the authors must indicate, unambiguously, which depolarization parameter are using. The volume depolarization ratio, δ, can still be used as a rough indicator of the presence of dust in the determination of the lidar ratio values. However, for aerosol classification in section 3 I strongly recommend using the aerosol linear depolarization ratio (δ_a), since it is an intrinsic property of aerosols and does not depend on the molecular*

25 *terms.* "

the reviewer correctly stresses a lack of clarity in the text, where in fact the parameters seem to be mixed. It is true that the aerosol depolarization can only be ascertained after the signal has been processed and then inverted in term of R, so that it cannot be used during the inversion. In our case the inversion of the LiDAR signal is accomplished with the Klett method

30 using piecewise constant extinction to backscatter ratio (LR) values, chosen accordingly to the volume depolarization (DR, in Rosati et al., 2016) and not aerosol depolarization, as would be proper to correctly discriminate among different classes of aerosol. However, when the aerosol load is significant – and these are the cases where an improper choice of LR would have more effect - the value of the volume tends to that of the aerosol depolarization, so that the use of the volume as a proxy of the aerosol in the inversion of the LiDAR signal can be accepted. We do not think it is worthwhile to dwell too much on that in

the text, but we need to remove the ambiguity in the text pointed out by the reviewer. To this aim we would then rewrite it as: (from 4,29 on) "... following the values reported in literature: using Volume depolarization as proxy of aerosol depolarization, highly depolarizing desert dust (δ (r) <10) is characterised by L...".

On the contrary, on page 6, line 34 we really meant Aerosol depolarization.

As the reviewer suggests, we expanded the discussion on inaccuracies in depolarization in (7,3...) as follows: "The reader should notice that the lower depolarization values that we observe respect what usually found in literature (especially for the dust layers) are likely linked to the calibration process, and in particular to the difficulty in individuating completely aerosol free layers in the vertical span of the adopted LiDAR system (from ground to 7 Km). In this work, depolarization has been calibrated following the "0° calibration" or the "atmospheric calibration" procedure, i.e. making use of a low aerosol height range in the lidar signal, where only the molecular contribution could be considered. There, the volume depolarization ratio has been forced to assume the well-known value of the air molecule linear depolarization ratio (Behrendt A. and Nakamura T. , 2002). We acknowledge that this calibration is unsatisfactory to produce quantitative results, as the possible residual presence of small amounts of highly depolarizing aerosol, in the assumed clean range, can easily compress the range of variability of the volume depolarization, and underestimate the final depolarization products (Freudenthaler et al. , 2009, 2016). However this possible source of inaccuracy does not compromise the purpose of this work."

" 3. Page 6, line 16. "For simplicity, dust on emissive areas is considered to be injected uniformly below 1000 m a.g.l., therefore only trajectories crossing this height are included in the footprint-emissions coupling". Is this a common procedure? Is there any previous work that backs this procedure? "

The choice of 1000m as a level for mineral dust injection is indeed a sharp assumption. We decided therefore to estimate the level of injection as the PBL top height, extracted by FLEXPART itself from the GFS input meteorological field (Stohl et al. , 2010), instead of adopting a fixed height. This does not significantly change the results of the analysis (see also answer to point 8)

" 4. Page 7, line 5: "The LiDAR classification, based on the statistical distribution of the overall observed δ_a and R values, is also applied here to overcome such limitations." However, in Fig. 1 it can be seen that the only parameter used for aerosol classification is δ. Because of this, we could get more information with a histogram of only δ values. Also, the figure should only show relevant δ values: more than half of the current figure corresponds to δ values (over 0.25) with almost no associated case. "

" 5. Page 7, line 13: [...] The authors are comparing their results to other references although they have previously said that their results might not match them due to calibration issues (again, this is likely due to a confusion between δ and δ_a). If δ is

finally used for the classification (although I strongly recommend δ_a), the threshold values should be derived from a statistical analysis of its value "

The distribution of δ_a and 1-1/R values (now Ra/(1+Ra)) is indeed what is really driving the aerosol classification. We agree with the review that was not clearly presented in the text and in Fig.1 of the manuscript. We corrected the text (from page 7, line 1: "Here we implement a three-types aerosol discrimination scheme to characterize the vertical and temporal aerosol variability over the region along the campaign period (15 June 2012 – 5 July 2012) based on the different statistical distribution of optical properties of each class (see Fig. 1). The reader should notice that [. . .]. The LiDAR classification, based on the statistical distribution of the overall observed δ_a and Ra values, is in fact applied here to overcome such limitations. The robustness of the results is then further supported by comparison with Lagrangian analysis and in-situ measurements.") and modified the axes of Fig.1. to magnify the region on which the values are mostly concentrated. It's easier now to identify the three different distributions of optical properties and the resulting classification. As is possible to see, each class shows a different range on the Ra/(1+Ra) parameter. We restricted therefore the threshold for classification on such intervals.

From (7,12): "The different aerosol classes can be discerned in three distinct patterns:

1. $0.1 < Ra/(Ra+1) < 0.8$ and low values of δ_a (< 3 %); such low values of aerosol linear depolarization ratio are indicative of spherical particles. These particles may be composed of anthropogenic pollution and, for higher values of Ra, by droplets, and are defined as non-depolarizing.

2. $0.3 < Ra/(Ra+1) < 0.7$ and high values of δ_a (> 10 %); In this class we find the highest values of aerosol linear depolarization ratio (mainly ranging from 10% to 20%) and this can be indicative of the presence of mineral dust particles. This class is defined as depolarizing.

3. $0.2 < Ra/(Ra+1) < 0.6$ and intermediate δ_a values (3 %< δ_a <10 %) which, based solely on Ra and δ_a, cannot be considered as indicative of a dominance of a defined aerosol type unless coupled to a more thorough correlation with additional observations. We will refer to this type as intermediate depolarizing.

"

As expected, the resulting aerosol mask (Fig.2) appears to be not meaningfully affected by such modification.

" 6. Figure 3. The relevant data in fig. 3 covers less than half of the total area and is hard to visualize. The figure should be redesigned for better interpretation. Also, it could be improved if the surface temperature were plot in an independent panel. "

As the purpose is to emphasize the evolution of meteorological conditions during the different phases of transport, we believe that it would be useful to represent the whole period in the same figure. We increased nevertheless the plot dimensions, to

facilitate the visualization of the main phases (as the dust transport events, that should be visible as variation in wind directions and increased wind intensity respect to the other days). Ground temperature is reported on a separate panel to improve the clarity of the figure.

" *7. Page 8, line 29 "Meteorological evolution is integrated with the aerosol optical variability from LiDAR (see Fig. 2) and with ground aerosol 30 number concentration and volume size distribution (estimated as the volume of a sphere of diameter corresponding to the volumeequivalent particle diameter) at SPC and CMN (see Fig. 4)" Meteorological parameters, lidar measurements, and in situ measurements are presented separately in different figures. They do not seem to be integrated.* "

What we meant here is that the results are derived from the addition and comparison of different information. To avoid confusion we changed the terminology from "Integrated" to "compared".

" *8. Page 10, line 18 "According to FLEXPART, the import of mineral dust persists until the morning of 23 June, when dust presence is not unambiguosly inferable from observations but the aerosol mask still indicates the presence of intermediate depolarizing particles below 2000 m. The second desert dust event predicted by FLEXPART shows the same timing with respect to observations but, while the APSS and the OPSS indicate a similar dust burden for the two desert aerosol advection events, the dust load indicated by the model(between 3 and 5 μgm^{-3}) appears lower respect to the previous events". In addition to limitations of the model, differences between estimations of FLEXPART over the SPC site at 1-2km and 3- 4km and surface-level measurements at SPC (different altitude level) or CMN (different location) might be partly caused by aerosol time-space variability. Have the authors considered a comparison against lidar-derived dust concentration? (These can be retrieved with the POLIPHON method by Mamouri [20142]).* "

The use of FLEXPART trajectories in this paper is serving as a support for assessing the nature of the observed particle layers. It is out of the scope of the study to provide an accurate estimate of the amount of dust transported, that would require indeed to take into account several possible sources of variability. Moreover, the possible inaccuracies on the aerosol depolarization values retrieval presented above, make difficult to apply the POLIPHON method properly. We believe that this would lead to an additional work that would go far beyond the purpose of the paper. We decided therefore to report dust air mass fraction evolution instead of the mineral dust reconstructed concentration, to avoid additional uncertainties coming from the estimate of the aerosol load, as rightly suggested by the reviewer. The information brought by such analysis, ancillary to the understanding of the nature of the layers observed by the LiDAR and in-situ measurements, remains mostly unchanged. The text on section 2.5 will be modified as follows: "To give an estimate of the variability in the mass of mineral dust advected over SPC we compute, for each release, the mass fraction of trajectories that encounter dust emissive regions respect to the total mass of the released cluster").

From (10,16): "Maximum mineral aerosol fraction from FLEXPART analysis occurs on June 20, both at the upper layer (9%) and at the bottom layer (9% also). According to FLEXPART, the import of mineral dust at the lower layer persists until the morning of 23 June, when dust presence is not unambiguously inferable from observations but the aerosol mask still indicates the presence of intermediate depolarizing particles below 2000 m. The second desert dust event predicted by FLEXPART again shows the same timing with respect to observation and also confirms the presence of a thick layer of dust that involves at the same time the 1000–2000 m and 3000–4000 m layers. The estimated mass fraction contribution on the contrary, especially in the lower layer (between 2 and 4 %), appears inferior respect to the previous events."

" 9. Figure 7. This figure does not seem to add any information to what can be seen in Fig. 6 and what is on the text. I think it can be removed. "

We agree that this information may be redundant, and we removed it from the manuscript.

" 10 .Issues regarding section 7:

Name of the section: "Effect of aerosol hygroscopic growth on aerosol particles light scattering and depolarization" -> Effect of aerosol hygroscopic growth scattering and depolarization "
Name of the section modified.

"Page 12, line 19. "LiDAR data (Fig. 2) frequently show, during early morning hours, a shallow layer of non-depolarizing aerosol below 300 m height, more easily visible during days characterized by desert dust and mixed dust events". Below 300 m the overlap of the lidar is not complete. Despite the authors claim that "Experimental correction allows the reconstruction of the LiDAR backscattering profile down to around 100 m, with an acceptable uncertainty (4-17)", they also say that "The reader should notice that the lower depolarization values that we observe respect what usually found in literature (especially for the dust layers) are more likely linked to the calibration process, and in particular to the difficulty in individuating completely aerosol free 5 layers in the vertical span of the adopted LiDAR system (from ground to 7 Km) (7-5)" The question is: to what extent can we trust depolarization measurements below complete overlap?"

For what concerns the uncertainties on the depolarization in the region of partial overlap, the Volume depolarization δ (being derived as a ratio of two signals both characterized by the same partial overlap loss) is not affected. Not so the δ_a, which is computed from δ and the total backscatter ratio (R), which can be impacted by systematic errors when retrieved in the partial overlap region. Errors on the R are discussed in Biavati et al. (2011), where the algorithm for partial overlap correction was presented; for the present work, the relative error on the reconstructed R remains below 10% in the altitude range where the correction has been applied. The relative error on the δ_a in the region of partial overlap decrease with increasing R and increase for increasing δ . For the values of δ that we found in our work, the error on δ_a remain below 15% for R greater than 1.5 and

below 30% for R greater than 1.25.

"*Figure 11 and Figure S2. For this kind of study it might be more appropriate to show the aerosol and humidity profiles at 5:00 UTC as regular plots (not color plots).*"

We modified the plots accordingly.

"*Page 12, line 29: [. . .]. In Fig. 11 and Fig. S2 we can see that in cases with presence of dust the depolarization decreases with RH. But this can be seen as the opposite: elevated dust layers (within dry hot airmasses from the Sahara) uncoupled from the PBL result in a decrease in the RH. In order to state that the dust depolarization properties are affected by the humidity, the authors should prove that a noticeable amount of dust actually reaches the lower altitudes where RH > 60 %. For instance, for the case used as example (30 June), at 5 UTC (time of the sounding) we do not see an especially high concentration of coarse particles at surface level compared to, for instance, 1 July (Fig. 4). Also, it would be interesting if the authors showed, in addition to the RH profile, the temperature profile for 30 June. This way we could see it a thermal inversion between the dust and the lower layers keeps them uncoupled. Finally, on 1 July we can see aerosols classified as dust reaching the surface (it is also the day with highest coarse-mode concentration at surface level). Although no soundings might be available at those times, it would be interesting to compare the depolarization values at the lowest altitudes available and the relative humidity at surface level.* "

We used the 30 June as a case example as in this day the effect of RH variation on the vertical profile of δ_a was particularly easy to individuate. In figure 1 we compare the δ_a and RH profiles with the potential temperature (TH) profile: in particular, in contrast to the nearly isothermal layer in correspondence of the core of the dust layer, we can notice that the δ_a depletion, and the RH sharp increase observed below 500 m, are associated to a notably more stable TH profile. In this case, nevertheless, we agree with the reviewer that the amount of dust at the ground was less meaningful than what observed during the 1 July, but indeed for this day we don't have the early morning radiosounding. We therefore report in figure 2 the temporal evolution of δ_a near ground (~ 150m) compared with RH and Temperatureat the ground. It is possible to notice the clear decrease of δ_a during the early hours of the morning, associated to high values of RH (higher than 70%) and low values of temperature (less than 25°C). During late afternoon this effect is less evident both because of less extreme values of RH and T and because of the deposition of coarser and more depolarizing particles (see for example Fig. 2 and Fig.4 of the manuscript). In the manuscript, for sake of completeness, we decided then to remove the single case study and discuss the vertical profiles of δ_a, TH and RH for dust and dust free days, where dust days corresponds to the days of increased coarse particles at the ground (from 20 to 22 June and from 30 June to 2 July). We discuss it on section 7, from (12,23) on.

Other comments, language errors and typos:

The manuscript was revised to fix language mistakes and typos.

Second reviewer:

General comments

5 " *[. . .]However, the main text of the manuscript needs to be more logically organized, and it is suggested to modify the logical structure of some sections to give clearer conclusions. For instance, the whole introduction part is in one large paragraph mentioning the characteristics of the Po river basin, previous studies over the Po Valley, mineral dust's adverse impact, and LiDAR observations, which is a little unclear. It is recommended to re-organize some of the sentences or separate this part into more than one paragraph and provide a clearer logical sequence introducing your study focus. For the conclusion part, it is*

10 *recommended to highlight a few key findings or conclusions using refined expression of the evidence.*"

We thanks the reviewer for the comment. We re-organized the manuscript introduction to have a clearer logical structure (presentation of the characteristics of the Po Valley, description on the possible sources of particulate over the region, goals, methods and focus of the study) and we introduced a sub-paragraph structure to separate the description of anthropogenic and

15 natural PM sources. Similarly, in the conclusions, we stressed the results in a clearer form. In particular:

We removed lines from (14,7) to (14,11).

From (14,21): "...carrying depolarizing aerosol.The study offered evidence of dust transport to the ground, showing clear

20 dust layers intrusion in the PBL and rapid mixing with local pollution. We showed how this mixed layer, generally characterized by lower depolarization values, can reach the ground within few hours and we showed, by direct comparison with ground in situ instruments, the corresponding enhancement of particle volume size distribution in the 2-5 μm range (leading to values higher than 1 $\mu m^3 cm^{-3}$)."

25 We substituted lines (14,30-31) with "The study revealed moreover the presence of events of late afternoon particles resuspension from the soil, not related to Saharan dust transport, impacting on the PM concentration near the ground. The existence of..."

From (15,6): "The combination of depolarization profiles with meteorological and aerosol measurements allowed also to

30 highlight the effects of the condition of high RH (typical for this region) on the particle processes. The analysis revealed how, in correspondence of a shallow layer near the ground (<500 m), in conditions of high relative humidity values ($RH > 60$ %), the aerosol linear depolarization ratio decreases respect to the above layer. Such effect is particularly visible when in presence of mineral dust particles near the ground ($delta_a$ decrease $\sim$3.5%). The temporal evolution and the high values of nitrates ion concentration (up to 18 μg m^{-3}) in the PM1 and PM10 channels during this period, suggest that the origin of such low

depolarization particles can be related to processes of secondary organic aerosol formation and hygroscopic growth on mineral dust particles with nitrate-enriched surface."

" *Finally, some language mistakes have been noticed and revision of the language is needed to give clearer meaning of the sentences. For instance: Page 3, line 15: '. . .basing on the analyses of continuous and vertically resolved particles light scattering and depolarization. . .' -> consider revising*"

5

We performed a revision of the manuscript to improve the clarity of the text as tracked in the revised version.

References

Behrendt A. and Nakamura T., 2002: Calculation of the calibration constant of polarization lidar and its dependency on atmospheric temperature. Opt. Express 10, 805-817.

Biavati, G., Donfrancesco, G., Cairo, F. and Feist, D.: Correction scheme for closerange lidar returns, Appl. Opt. 50, 5872-5882, 2011.

5 Freudenthaler, V., Esselborn, M., Wiegner, M., Heese, B., Tesche, M., Ansmann, A., Müller, D., Althausen, D., Wirth, M., Fix, A., Ehret, G., Knippertz, P., Toledano, C., Gasteiger, J., Garhammer, M., and Seefeldner, M.: Depolarization ratio profiling at several wavelengths in pure Saharan dust during SAMUM 2006, Tellus B, 61, 165–179, 2009.

Freudenthaler, V.: About the effects of polarising optics on lidar signals and the Δ90 calibration, Atmos. Meas. Tech., 9, 4181-4255, https://doi.org/10.5194/amt-9-4181- 2016, 2016.

10 Stohl, A., Sodemann, H., Eckhardt, S., Frank, A., Seibert, P., Wotawa, G., Morton, D., Arnold, D. and Harustak, M.: The Lagrangian particle dispersion model FLEXPART version 9.3, Tech. rep., Norwegian Institute of Air Research (NILU), Kjeller, Norway, available at: http://flexpart.eu, last access: 2 June 2016, 2010.
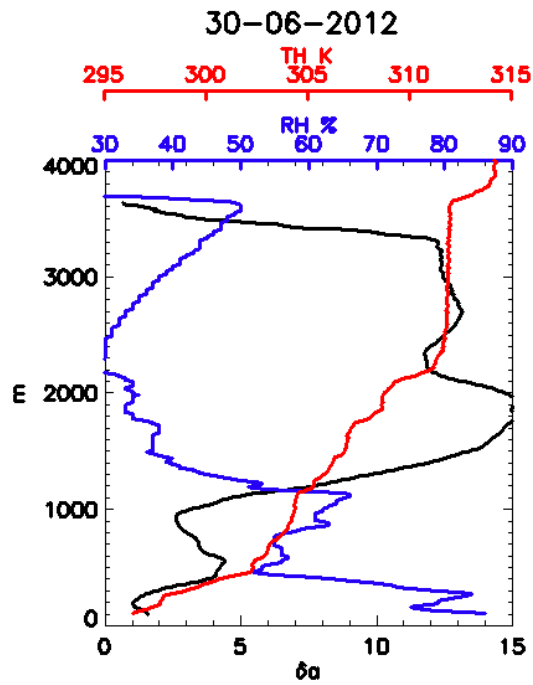
Figure 1. Vertical profiles of $delta_a$ (black), TH (red) and RH (blue) for 30 June, 05:00 UTC.
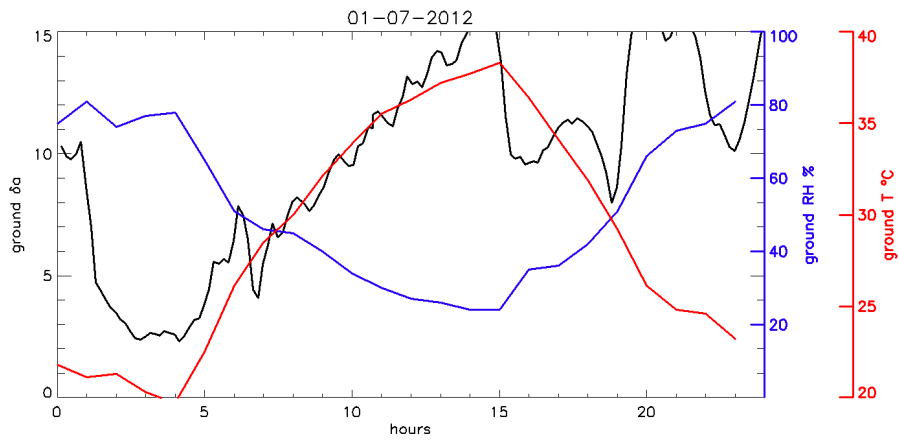

Figure 2. Temporal evolution of $delta_a$ (black) at 150m, and TH (red) and RH (blue) at the ground, 1 July case study

Vertical distribution of aerosol optical properties in the Po Valley during the 2012 summer campaigns

Silvia Bucci[1,2], Paolo Cristofanelli[3], Stefano Decesari[3], Angela Marinoni[3], Silvia Sandrini[3], Johannes Größ[4], Alfred Wiedensohler[4], Chiara F. Di Marco[5], Eiko Nemitz[5], Francesco Cairo[1], Luca Di Liberto[1], and Federico Fierli[1]

[1]Institute for Atmospheric Sciences and Climate of the National Research Council , (ISAC-CNR), Rome, Italy
[2]Sc Dept. of Physics, Ferrara University, Ferrara, Italy
[3]Institute for Atmospheric Sciences and Climate of the National Research Council, (ISAC-CNR), Bologna, Italy
[4]Leibniz Institute for Tropospheric Research, Leipzig, Germany
[5]Natural Environment Research Council, Centre for Ecology & Hydrology, Penicuik, UK

Correspondence: Federico Fierli (f.fierli@isac.cnr.it), Silvia Bucci (s.bucci@isac.cnr.it)

Abstract. Studying the vertical distribution of aerosol ~~particles~~ particle physical and chemical properties in the troposphere is essential to understand the relative importance of local ~~emissions~~ emission processes vs. long-range transport on column-integrated aerosol properties (e.g. the aerosol optical depth (AOD), affecting regional climate) as well as on the aerosol burden and its impacts on air quality at the ground. The main objective of this paper is to investigate the transport of desert dust in the middle troposphere and its intrusion into the planetary boundary layer (PBL) over the Po Valley (Italy), a region considered one of the major European pollution hot-spots for the frequency of particulate matter (PM) limit values exceedances. Events of mineral aerosol uplift from local (soil) sources and phenomena of hygroscopic growth at the ground are also investigated, possibly affecting the PM concentration in the region as well. During the PEGASOS 2012 field campaign, an integrated observing-modeling system was set up based on near-surface measurements (particle concentration and chemistry), vertical profiling (backscatter coefficient profiles from LiDAR and radiosoundings) and Lagrangian air masses transport simulations by FLEXPART model. Measurements were taken at the San Pietro Capofiume supersite (44°39' N, 11°37' 0 E, 11 m a.s.l), located in a rural area relatively close to some major urban and industrial emissive areas in the Po Valley. Mt. Cimone (44°12' N, 10°42' E, 2165 m a.s.l.) WMO/GAW station observations are also included in the study to characterize regional-scale variability. Results show that, in the Po Valley, aerosol is detected mainly below 2000 m a.s.l. with a prevalent occurrence of non-depolarizing particles (> 50 % throughout the campaign) and a vertical distribution modulated by the PBL daily evolution. Two intense events of mineral dust transport from Northern Africa (19–21 June and 29 June to 2 July) are observed, with layers advected mainly above 2000 m height, but lately sinking and mixing in the PBL. As a consequence, a non-negligible occurrence of mineral dust is observed close to the ground (∼ 7 % of occurrence during a 1-month campaign). The observations unambiguously show Saharan dust layers intruding the Po Valley ~~summertime~~ mixing layer and directly affecting the aerosol concentrations near the surface. Finally, LiDAR observations indicate also strong variability in aerosol on shorter timescales (hourly) highlighting: a) events of hygroscopic growth of anthropogenic aerosol, visible ~~in~~ as shallow layers of low depolarization near the ground. Such events are identified during early morning hours at high relative humidity (RH) conditions (RH >

1

80 %). The process is observed concurrently with high PM1 nitrate concentration (up to 15 μg cm^{-3}), hence mainly explicable by deliquescence of fine anthropogenic particles, and during mineral dust intrusion episodes, when water condensation on dust particles could instead represent the dominant contribution; b) frequent events (mean diurnal occurrence of ∼22% during the whole campaign) of rapid uplift of mineral depolarizing particles in afternoon-evening hours up to 2000 m a.s.l. height. The origin of such particles cannot be directly related to long-range transport events, being instead likely linked to processes of soil particles resuspension from agricultural lands.

1 Introduction

The Po river basin in Northern Italy is one of the most important emissive area in Europe, characterized by high concentration of both natural and anthropogenic aerosol and trace gases (Monks et al., 2009). The geographical location of this region, surrounded by two mountain ranges, promotes frequent occurrence of stagnant meteorological conditions (Rossa et al., 2012), with accumulation of local pollution (Hanke et al., 2003; Crosier et al., 2007; Saarikoski et al., 2012; Decesari et al., 2014) from industrial, urban and agricultural emissions, and complex processes of aerosol-chemicals transformation. At the same time, the relative proximity to the Sahara desert, that represents the major mineral dust source of the planet (Prospero et al., 2002; Washington et al., 2003), makes this region subject to long range mineral dust transport, especially during the summer season (Kalivitis et al., 2007; Marinoni et al., 2008; Pederzoli et al., 2010; Carnevale et al., 2012). Such combination leads to unusually high concentrations of atmospheric pollutants and particulate matter, with frequent and prolonged periods of intense pollution. The large amount of people living in the region (more than 20M potentially exposed to high pollution levels) accentuates the need of accurate studies on particulate variability over the Po Valley. Observations show that the spatial distribution and composition of aerosol over the area is often complex and variable in space and time, due to the interplay of sources and transport regimes (Lelieveld et al., 2002).

- *Local anthropogenic sources.* The co-emission of particles and NOx from combustion emissions and the widespread sources of ammonia from agricultural activities over the region (Clarisse et al., 2009) lead to the accumulation of primary carbonaceous particles and secondary inorganic aerosols (ammonium nitrate) in the lower layers of the atmosphere. Crosier et al. (2007), during a campaign in summer 2004, observed that, under easterly flow, ammonium sulphate and organics dominated the sub-micron aerosol particle fraction while, under westerly anticyclonic flow, the large NOx and ammonium emissions at the surface resulted in a large ammonium nitrate concentration in air masses recirculating over the Po Valley. During summer 2012, under similar meteorological features (anticyclonic conditions and PBL air recirculation), Sandrini et al. (2016) observed a significant enhancement of secondary organic and inorganic aerosol particle mass. They also pointed out differences in rural and urban area aerosol behaviour: rural area, being characterized during nightareas, during night, were characterized by higher relative humidity and lower temperature compared to the urban one, and showed higher fine nitrate nocturnal concentration and formation of ammonium nitrate in the large accumulation mode aerosol (0.42-1.2 μm). This large amount of highly hydrophilic compounds significantly increase particles aerosol particle light scattering due to additional water uptake: ammonium nitrate-rich

particles are very hydrophilic and, in conjunction with the high relative humidity conditions often encountered in the Po Valley floor, contribute to the build-up of hazes in the region, also in the summer season (Hodas et al., 2014). ~~At the same time, the relative proximity to the Sahara desert, that represents the major mineral dust source of the planet (Prospero et al., 2002; Washington et al., 2003) , makes this region subject to long range mineral dust transport, especially during the summer season (Kalivitis et al., 2007; Marinoni et al., 2008; Pederzoli et al., 2010; Carnevale et al., 2012) . Saharan~~

- *Long range natural sources: Saharan dust transport.* Mineral dust intrusion episodes can significantly affect public health: epidemiological studies on Italy (Sajani et al. (2010)) revealed increased respiratory mortality in correspondence of such events. During summer months, saharan dust particles are uplifted to the mid-troposphere levels (up to 5 km) by the strong surface winds and the large-scale convection that typically involves north Sahara ~~during the summer months~~ in this season (Querol et al., 2009a). Mineral dust is then transported over the whole Mediterranean basin, following usually anticyclonic pattern of circulation (Gkikas et al., 2013) triggered by the extended subtropical anticyclone of the Atlantic Azores. Mineral dust over the Mediterranean is found to be usually transported in the lower free troposphere between 2 and 5 km of altitude (Papayannis et al., 2005; Kalivitis et al., 2007); nevertheless, there is indication of episodes of mixing with PBL air (Bonasoni et al., 2004; Perrino et al., 2008; Pederzoli et al., 2010), with ~~an estimated~~ a contribution to the surface particulate mass concentration estimated to be of the order of 10 µg m^{-3}. ~~Such~~ While the above mentioned studies rely on in situ measurements, ~~while~~ a direct evidence of mineral dust entrainment in the PBL from continuous vertically resolved observations over the Po Valley is still lacking. ~~In this paper, to improve the understanding of the impact of such processes, we provide direct evidence of dust penetration in the lower troposphere of Po Valley, a characterization of timing and vertical extent of its mixing with local pollution, and a direct comparison between low level intrusion and the particles concentration enhancement at the ground. Mineral dust intrusion events can indeed significantly affect public health: epidemiological studies on Italy (Sajani et al. (2010)) revealed increased respiratory mortality in correspondence of dust transport over the region. More in general, as~~

As accumulation of pollution can affect both regional climate and public health (Lelieveld et al., 2002; Kanakidou et al., , 2011), a better understanding on the processes contributing to the high concentration of PM on the region is needed. The present paper offers more details on aerosol processes related to both local and long-range ~~aerosol processes basing~~ sources, and their interaction, in the Po Valley region. The study is based on the analyses of continuous and vertically resolved ~~particles~~ profiles of particle light scattering and depolarization~~in the Po Valley~~: in particular, it exploits Light Detection and Ranging o Laser Imaging Detection and Ranging (LiDAR) aerosol characterization, assisted by ground observations and transport models, ~~are exploited~~ to identify the origin of the particulate entering and mixing in the PBL during summer season. The LiDAR represents a widely used technique for studying the vertical and temporal distribution of particulate matter optical properties (e.g., Hamonou et al., 1999; Matthias et al., 2002; Dulac and Chazette, 2013; Pappalardo et al., 2004; Amiridis et al., 2005; Papayannis et al., 2005; Flentje et al., 2010b). Coupled with in situ observations and model analysis, LiDAR observations can also be used to derive transport pathways and physical-chemical processes (e.g., Papayannis et al., 2005; Größ et al., 2013). In

this work, LiDAR observations are ~~integrated~~ compared with near surface measurement techniques from ~~observation~~ sites at different altitudes, and ~~coupled with~~ supported by Lagrangian model simulations, to provide new insights on the processes that affect aerosol particle variability in the Po Valley ~~, improving~~ and improve the understanding on the possible role of different local and remote sources on the PM level over the region. The focus is on the observation of mineral aerosol in the PBL, on the analysis of its origins and on its mixing and interaction with local aerosol particles and anthropogenic pollution. Please note that, from here on, by "aerosol" we will refer to just the aerosol particle phase, excluding the carrier gas.

2 Observations and methodology

Observations were performed in the framework of the SuperSito project, coordinated by the Regional Agency of Prevention and Environment and funded by Region Emilia-Romagna (ARPA-ER, Italy www.supersito-er.it), and of the FP7 European project PEGASOS (Pan-European Gas-AeroSOl-climate interaction Study, pegasos.iceht.forth.gr).

2.1 Measurement stations

The San Pietro Capofiume (hereafter SPC) station (44°39' N, 11°37' 0 E, 11 m a.s.l) is located in the South-Eastern part of the Po Valley, at a flat rural background site relatively close to densely populated cities and industrial sites (i.e. 30 km NE from Bologna urban area, with about 0.5 M inhabitants, and 20 km S from Ferrara, with 0.15 M inhabitants). SPC is included in the list of WMO/GAW regional stations, being representative of the surrounding wider region. The Mt. Cimone (44°12' N, 10°42' E, 2165 m) WMO/GAW global station (hereafter CMN), located 100 km south-west from SPC, is instead situated at the top of the highest peak of the Northern Apennines. For the ~~most~~ greater part of the year, CMN observations can be considered representative of the background conditions of the South Europe free troposphere (Bonasoni et al., 2000a), while, during warm months, it can be considered at a transition level between the uplifted boundary layer and the free troposphere (Andrews et al., 2011). Under summer anticyclonic conditions, polluted air masses transport from the regional boundary layer can be detected at CMN, due to thermal transport processes and PBL growth (Marinoni et al., 2008; Cristofanelli et al., 2013). CMN also represents the first mountain ridge impacted by Saharan air masses on their way across the Central Mediterranean basin to Europe.

2.2 Aerosol ~~particles~~ particle light backscattering coefficient profiles: LiDAR observations

The LiDAR system operating in SPC, described in Cairo et al. (2012), uses a 532 nm Nd-YAG pulsed laser source, with pulse duration of 1 ns, 400 µJ of energy and repetition rate of 1 kHz. The optical receiver of the LiDAR is a Newtonian telescope. Taking into account the distance between the telescope and the laser beam, the overlap of the laser within the FOV begins at few tens of meters (around 50 m) from the system, and is complete at around 300 m. Experimental correction allows the reconstruction of the LiDAR backscattering profile down to around 100 m, with an acceptable uncertainty (close to 10 %) on the backscatter ratio precision (see Rosati et al., 2016, and its supplementary material). Profiles are collected every 10 minutes with a vertical resolution of 7.5 m extending, on average, up to 7 km. In the following discussion, we will make use of ~~backscattering ratio~~

~~(R) and aerosol depolarization (δa~~the aerosol linear depolarization ratio (δa) and the aerosol backscattering ratio $Ra = R - 1$ derived from the total backscattering ratio (R)), defined as ~~(Browell et al., 1990; Cairo et al., 1999)~~ (Cairo et al., 1999; Browell et al., 1990)

$$\delta_a \approx \frac{\beta_{a_{perp}}}{\beta_{a_{par}}}$$

$$R(r) = \frac{\beta_a(r) + \beta_m(r)}{\beta_m(r)} \delta_a =$$

5 and therefore

$$Ra(r) = R(r) - 1 = \frac{\beta_a(r)}{\beta_m(r)}$$

$\beta_m(r)$ represents the backscatter coefficient from molecular contribution while $\beta_{a_{perp}}$ and $\beta_{a_{par}}$ ~~represent~~ are the backscattered signal components from aerosol particle light scattering, with polarization respectively perpendicular and parallel to the polarization of the emitted light. The inversion of the LiDAR signal is accomplished with the Klett method (Klett, 1985; Fernald

10 , 1984), finding a suitable region of the profile that is supposed to be free of aerosol to calibrate the signal, and using piecewise constant extinction-to backscattering ratio (LiDAR ratio, ~~L~~LR) values. ~~We make use of~~Using volume depolarization ($\delta(r)$, see Cairo et al. (2012)) as proxy of aerosol linear depolarization ratio, we select different values for ~~L~~LR following what reported in literature: highly depolarizing desert dust (~~identified by $\delta_a(r) > 10\%$) is characterized by~~ L $\delta(r) < 10\%$) is associated to a LR equal to 50 sr (Müller et al., 2007) while for low depolarizing aerosol we assume the values typical for anthropogenic

15 aerosol, ~~L~~LR∼60–70 sr (Murayama et al., 1999; Ferrare et al., 2001; Fiebig et al., 2002). In addition we considered different values for water cloud (~~L = 20~~LR = 20 sr) and ice clouds (~~L = 30~~LR = 30 sr) (Chen et al., 2002; O'Connor et al., 2004). A more detailed description of the methods used to perform the inversion of LiDAR data, together with a through uncertainty analysis, performance in conditions close to the SPC site and additional experimental set-up details, are given in Cairo et al. (2012) and Rosati et al. (2016) and its supplementary material.

20 ## 2.3 Aerosol ~~particles~~ particle number size distribution: APSS and OPSS

Aerosol concentrations at the ground are obtained from an Aerodynamic Particle Sizer Spectrometer (Type TSI, APS model 3321), operating at SPC, that provides real-time aerodynamic measurements of particles from 0.5 to 10 μm at 1 minute time resolution. The aerodynamic diameter is defined as the physical diameter that a unit density sphere will have if settles through the air with a velocity equal to the one of the sampled particle. The aerodynamic diameters of particles is established measuring

25 their transit time between two points when accelerated singly through a well-defined flow field. The aerodynamic diameters are here converted to volume-equivalent particle diameters, following Khlystov et al. (2004) and assuming an effective ~~particles~~ particle density of 1.8, during dust days, and 1.55 during the remaining days, accordingly to the values retrieved by Putaud et al. (2004). The near surface aerosol number concentrations at the free tropospheric level are instead derived from an Optical Particle Size Spectrometer (Type Grimm, OPSS Particle Size Analyser Mod. 1.108) operating at the CMN station. The OPSS

provides particle counts in the ~~diameters~~ diameter (Dp) range of $0.3\mu m < Dp < 10\mu m$. The instrument is based on the quantification of the 90° scattering of light by aerosol. According to the specifications, the reproducibility of the OPSS in particle counts is $\pm 2\%$ (Putaud et al., 2004). Such measurements allow the determination of the fine ($0.3\mu m < Dp < 1\mu m$) and coarse ($1\mu m < Dp < 10\mu m$) aerosol fractions with a 1 minute time resolution. For the purpose of the paper we make use of the time

5   series of coarse ($Dp > 1\mu m$) aerosol concentration observed at CMN, without any further correction to the "optical" diameter, to provide a clear indication on the presence of mineral dust layer in the free troposphere (Marinoni et al., 2008; Duchi et al., 2016).

2.4 Chemical Composition: MARGA

The Monitor for AeRosol and GAses (MARGA, Metrohm Applikon B.V. Schiedam NL) is a wet chemistry instrument that

10   provides continuous measurements of the water soluble inorganic gases and aerosol components that might have a direct effect on air quality (Makkonen et al., 2012; Rumsey et al., 2014). The analytical system allows for the characterization of inorganic aerosol ($Cl^-, NO_3^-, SO_4^{2-}, NH_4^+, K^+, Ca^{2+}, Mg^{2+}, Na^+$) and gases ($NH_3, HNO_3, SO_2, HONO, HCl$) at hourly resolution (Twigg et al. , 2015). In the sampling box, the air passes through a Wet Rotating Denuder (WRD) (Keuken et al., 1988) where water soluble gases are stripped from the air stream and collected in water. The sampled air then continues

15   through a Steam-Jet Aerosol Collector (SJAC, Khlystov et al., 1995; Slanina et al., 2001) where the water soluble aerosols are separated from the air stream and collected. The gas and aerosol samples are then analysed by online ion chromatography with high ~~accuracies~~ accuracy (detection limits as low as 0.01 µg m^{-3} (Twigg et al. , 2015)). Size-selective particle cyclones are used in front of the two MARGA sampling boxes so that the size of the particles for analysis can be limited to an aerodynamic diameter of less than 10 (PM10) or 1 (PM1) µm.

20 ## 2.5 Transport modelling

We make use of the FLEXPART Lagrangian particle dispersion model (version 9.02)(Stohl et al., 2005, and references therein) to characterize the transport during ~~summer 2012 (Stohl et al., 2005, and references therein)~~ the campaign period. FLEXPART is a widely used model system to simulate synoptic and mesoscale transport and diffusion of aerosol and trace gases, as well as loss processes such as dry and wet deposition or radioactive decay (Stohl et al., 2005), and has been validated using

25   large-scale tracer experiments (Stohl et al., 1998; Forster et al., 2007). In our case, the model is driven by pressure level data from NCEP Global Forecast System (GFS) (rda.ucar.edu). Meteorological input is provided ~~each~~ every 6 hours (00:00, 06:00, 12:00 and 18:00 UTC) at a resolution of $0.5° \times 0.5°$. ~~To assess the effective role of Saharan dust transport on aerosol concentration over Northern Italy, 5-days backward plumes are coupled with mineral dust emissions from Africa taken from the DREAM inventory (???, website http://www.bsc.es/earth-sciences/mineral-dust-forecast-system/bsc-dream8b-forecast) at~~

30   ~~0.2° × 0.2° horizontal resolution. FLEXPART gives as output~~ FLEXPART output is the footprint of the retroplume, namely the time of residence of the air parcels over each geographical grid point ~~,~~ during the 5 days prior to the moment of the trajectories release. Such quantity, expressed in seconds, gives an indication of which ~~, and in which extent,~~ emissive regions are going to contribute (and in which extent) to the mineral dust enrichment of the air parcels, influencing therefore dust burden

at the time and position of trajectories release. ~~The product of the footprint with the dust emission rate (given in) is then integrated over the whole geographical domain to~~ To give an estimate of the variability in the mass of mineral dust advected over SPC~~for each back-plume release. For simplicity, dust on emissive areas~~, we compute, for each release, the mass fraction of trajectories that encounter dust emissive regions respect to the total mass of the released cluster. Dust is considered to be injected ~~uniformly below 1000 a.g.l., therefore only trajectories crossing this height are included in the footprint-emissions coupling. The backtrajectories~~ in the atmosphere when the trajectories are crossing the PBL height (as extracted by FLEXPART itself from the GFS input meteorological field, see Stohl et al. (2010)) over the Sahara desert. The backtrajectory clusters were released every 6 hours, along the whole campaign period, from the SPC station in correspondence of the $1000 - 2000$ m and $3000 - 4000$ m atmospheric layers.

3 LiDAR aerosol type classification

LiDAR observations have been extensively used to identify mineral dust layers and discriminate among different typologies of aerosols, based on a choice of specific ranges of optical parameters considered representatives of distinct aerosol types. Examples are shown in Burton et al. (2012), where the classification among eight different types of aerosol is derived from ~~total volume~~ depolarization ratio (δ), LiDAR ratio (LR) and the color ratio (CR). In Größ et al. (2013) the categorized aerosol types are: sea-salt, mineral dust and mixed dust based on LR and aerosol ~~depolarization~~ linear depolarization ratio δ_a. The estimate of LR (that requires an independent information on the extinction that should be derived from the Raman signal), as well as an evaluation of the CR (based on the adoption of two wavelength channel), is not possible with single wavelength elastic LiDAR as the one deployed at SPC during the PEGASOS campaign. Nevertheless, some typologies of aerosol show distinct values of aerosol ~~depolarization~~ linear depolarization ratio. At 532 nm, values of ~~aerosol depolarization~~ δ_a around or higher than 30 % are generally associated with layers of nearly pure mineral dust while smaller values (around 8–10 %) are often detected in correspondence of mixture of mineral dust and non-depolarizing particles (Murayama et al., 2003; Sugimoto et al., 2006; Tesche et al., 2009a). By contrast, smoke and other anthropogenic aerosols exhibit low values of ~~aerosol depolarization~~ δ_a (less than 5 %)(Sun et al., 2012; Größ et al., 2013).

~~Following the results of the abovementioned studies, here~~ Here we implement a three-types aerosol discrimination scheme, based on the different statistical distribution of optical properties of each class (see Fig. 1), to characterize the vertical and temporal aerosol variability over the region along the campaign period (15 June 2012 – 5 July 2012). The reader should notice that the lower ~~depolarization~~ δ_a values that we observe ~~respect~~ with respect to what usually found in literature (especially for the dust layers) are ~~more~~ likely linked to the calibration process, and in particular to the difficulty in individuating completely aerosol free layers in the vertical span of the adopted LiDAR system (from the ground to 7 ~~Km).~~ Km). In this work, δ has been calibrated following the "0° calibration" or the "atmospheric calibration" procedure, i.e. making use of a low aerosol height range in the LiDAR signal, where only the molecular contribution could be considered. There, the volume depolarization ratio has been forced to assume the well-known value of the air molecule linear depolarization ratio (Behrendt and Nakamura , 2002) . We acknowledge that this calibration is unsatisfactory to produce quantitative results, as the

possible residual presence of small amounts of highly depolarizing aerosol, in the assumed clean range, can easily compress the range of variability of the volume depolarization, and underestimate the final depolarization products (Freudenthaler et al., 2009, 2016) . However this possible source of inaccuracy does not compromise the purpose of this work. The LiDAR classification, based on the statistical distribution of the overall observed δ_a and ~~R~~ Ra values, is ~~also~~ in fact applied here to overcome such lim-

5   itations. The robustness of the results are then further supported by comparison with lagrangian analysis and ~~in-situ~~ in situ measurements.

Figure 1 reports the probability density function, along the whole measurements campaign, of the aerosol occurrence, expressed as a function of ~~$1-1/R$~~ $Ra/(Ra+1)$ (ranging from 0 ~~,~~ in aerosol free condition, i.e. $R_a = 0$, to 1 ~~when R~~ in presence of an opaque aerosol layer, when Ra tends to infinity) and δ_a. The analysis includes 10 minutes resolution observations from

10   the ground up to 5000 m height, for a total of about $1.5 \cdot 10^7$ sampling points. ~~Aerosol, identified with values of $1-1/R$ larger than 0.2, can be further~~ The different aerosol classes can be discerned in three distinct patterns:

1. $0.1 < Ra/(Ra+1) < 0.8$ and low values of δ_a (< 3 %); ~~based on the above references, these~~ such low values of aerosol linear depolarization ratio are indicative of spherical particles. These particles may be composed of anthropogenic pollution and, for higher values of ~~R~~ Ra, by droplets, and are defined as non-depolarizing.

15   2. $0.3 < Ra/(Ra+1) < 0.7$ and high values of δ_a (> 10 %); ~~according to the previously mentioned literature,~~ In this class we find the highest values of aerosol linear depolarization ratio (mainly ranging from 10% to 20%) and this can be ~~consider as a threshold value for mineral dust or mixed dust~~ indicative of the presence of mineral dust particles. This class is defined as depolarizing.

3. $0.2 < Ra/(Ra+1) < 0.6$ and intermediate δ_a values (3 %< δ_a <10 %) which, based solely on ~~R~~ Ra and δ_a, cannot be

20   considered as indicative of a dominance of a defined aerosol type unless coupled to a more thorough correlation with additional observations. We will refer to this type as intermediate depolarizing.

The boxes in Fig. 1 ~~report the R~~ delimit the $Ra/(Ra+1)$ and δ_a ranges for each of the three classes used to derive the aerosol mask for the whole campaign. The results are reported in Fig. 2 together with the profiles of ~~scattering ratio R and aerosol depolarization~~ $Ra/(Ra+1)$ and aerosol linear depolarization ratio δ_a. Overall, non-depolarizing particles (type 1) are

25   dominant throughout the campaign with a total occurrence of 49 % of the measurements in the 100-5000 m range. They are observed prevalently below 2000 m height, and are associated with enhanced values of ~~R (parameter $1-1/R$~~ Ra ($Ra/(Ra+1)$ ranging between 0.3 and 0.6). Due to the presence of such particles, the vertical gradient of ~~R~~ Ra marks, when not masked by the presence of mineral dust layers or clouds, the PBL evolution. Two events of depolarizing aerosol (19 June – 21 June and 29 June – 02 July), recognized as type 2 and likely related to mineral dust presence, are observed between 2000 m and 5000

30   m. Such events are also clearly visible as enhancement of ~~R~~ Ra in the free troposphere with values of ~~$1-1/R$~~ $Ra/(Ra+1)$ ranging from 0.6 and 0.8. The intermediate class (detected with an occurrence of around 19 % during the whole campaign) is found in close proximity of the depolarizing aerosol and within the PBL. The observed vertical and time distribution of these intermediate type particles indicates the possibility of mixing of the dust depolarizing layers with local non-depolarizing particulate. Nevertheless, intermediate δ_a values are also observed systematically after 12:00 UTC (Universal Time Coordinate),

between 0 and 1500 m height, for the majority of dust-free days. The nature of such intermediate non-dust depolarizing aerosol is further discussed in Sect. 6.

4 Meteorology and synoptic aerosol regimes

The evolution of the meteorological conditions at SPC is reported in Fig. 3. Vertical profiles from the ground up to 4 km height of wind speed and direction come from radiosondes (Vaisala RS92) launched daily at 00:00, 06:00 and 12:00 UTC. ~~Figure~~ Panel c of Fig. 3 reports also the evolution of ground temperature at 12:00 UTC. PBL evolution description is referred to the PBL height time series presented in Sandrini et al. (2016) and reported also in the supplementary material (see Fig. S1). The observation of wind profiles over SPC highlights a sequence of distinct meteorological regimes:

- Stagnation period: (15 June – 19 June) This first phase is characterised by a situation of stagnant conditions (wind speed less than $4 \, \mathrm{m \, s^{-1}}$ below 2000 m height) with a progressive warming of the air masses (from 29 °C up to 34 °C at the ground). The PBL top is limited below 1500 m until 19th June when it ~~reached~~ reaches 2000 m.

- South-westerly winds: (20 June – 21 June) During this phase higher wind speeds (between $11 \, \mathrm{m \, s^{-1}}$ and $16 \, \mathrm{m \, s^{-1}}$) are observed above 2000 m. Correspondingly, wind direction profiles indicate a prevalent South and South-West provenience. The arrival of warm Saharan air masses (temperature at the ground around 32°C–33°C) ~~led~~ leads to a more intense PBL development (up to 2000m) respect to the previous stagnation phase. (30 June – 5 July) During the last days of the campaign, strong winds (between 12 and $15 \, \mathrm{m \, s^{-1}}$ with a peak of $20 \, \mathrm{m \, s^{-1}}$ on 3 July) are observed above 1500 m. While during ~~the~~ 30 June winds are coming mainly from South, the following days are characterized by a steering to ~~south westerly~~ south-westerly (1 July) and then westerly flow (2 and 3 July). During this phase, ~~temperatures~~ temperature at the ground ~~reached 34~~ reaches its highest values (35°C~~–35~~–37°C) but the dust layer presence made it difficult to ~~unambiguosly~~ unambiguously retrieve the PBL top. During the ~~immediatly~~ immediately following days (3–4 July), the PBL top was detected ~~to be~~ above 2000m.

- North-easterly winds: (22 June – 29 June) The radiosounding profiles indicate a prevalence of south-easterly or easterly winds above 2000 m a.g.l.. Northerly/north-easterly winds are instead often visible at lower altitudes, in particular between 23 and 24 June below 1000 m, on 26 June below 500 m (associated also to wind intensities up to $10 \, \mathrm{m \, s^{-1}}$) and on 27 June between 500 m and 1800 m. During this period, ground ~~temperatures first decrease to 30~~ temperature first decreases to 28 °C then ~~increase again after 27 June, up to 33~~ increases again after 26 June, reaching 35 °C on 29 June. The PBL maximum height varies between 1500 m and 2000 m a.g.l.. Such conditions are favourable for the export of the Po Valley pollution toward the Tyrrhenian Sea and will be extensively discussed in a companion paper.

The evolution of the observed size distribution and optical classification during the distinct meteorological regimes is presented in the following sections.

4.1 Summer stagnant conditions: 15–19 June

Meteorological evolution is ~~integrated~~ compared with the aerosol optical variability from LiDAR (see Fig. 2) and with ground aerosol number concentration and volume size distribution (estimated as the volume of a sphere ~~of~~ with diameter corresponding to the volume-equivalent particle diameter) at SPC and CMN (see Fig. 4). Panel a of Fig. 4 shows the time trend of small

5   ~~particles~~ particle concentration ($297\,\mathrm{nm} < Dp < 420\,\mathrm{nm}$) from the APSS at SPC. The stagnation period (15–19 June), typical for the Po Valley on hot summer days (Rossa et al., 2012), is characterized by a marked daily cycle in the aerosol concentration and by a progressive day-by-day accumulation of particles in the PBL. This is noticeable in the increase of the particle number size distribution of small particles from APSS (from $5\,\mathrm{cm}^{-3}$ to nearly $20\,\mathrm{cm}^{-3}$) during the early morning hours (00:00-06:00 UTC), when the lower troposphere is stably stratified. The LiDAR observations (Fig. 2) show a persistent layer of non-

10   depolarizing particles up to $2\,\mathrm{km}$ height, attributable to anthropogenic aerosol and modulated vertically by the PBL daily cycle. APSS data in panel b of Fig. 4 show a bimodal aerosol distribution with a clear increase of volume mode due to submicron particles ($0.5\,\mathrm{\mu m} < Dp < 1\,\mathrm{\mu m}$) growing from $0.4\,\mathrm{\mu m^3 cm^{-3}}$ to more than $1\,\mathrm{\mu m^3 cm^{-3}}$. During this period of the campaign, the OPSS at CMN (panel c Fig. 4) indicates coarse particle number concentrations below $0.4\,\mathrm{cm}^{-3}$.

4.2 Saharan dust events: 19–21 June and ~~28~~ 29 June–3 July

15   During the first event (19 to 21 June) strong south-westerly winds (with speeds greater than $10\,\mathrm{m\,s}^{-1}$ above $2000\,\mathrm{m}$ height) are associated with a stable anticyclonic circulation centred above South Mediterranean and Tunisia, leading to ~~efficient south-south westerly~~ an efficient south/south-westerly circulation. Mineral dust can be clearly observed as an enhancement in LiDAR ~~R~~ Ra profiles (Fig. 2, panel b) above $2000\,\mathrm{m}$ until June 21 while, below that height, it is not possible to discern any deviation from the background aerosol signal. The enhancement in ~~R~~ Ra is accompanied with increased aerosol ~~depolarization~~

20   linear depolarization ratio ($\delta_a \sim 10\% - 15\%$) during the whole event, with values up to $20\,\%$ above $3000\,\mathrm{m}$ during ~~the~~ 20 June, resulting in a coherent layer of type 2 particles visible in the aerosol mask (panel a of Fig. 2). In correspondence of the presence of dust aerosol at $2000\,\mathrm{m}$ level, the OPSS at CMN (panel c, Fig. 4) detects an increase of coarse ~~particles~~ particle concentration up to $1.8\,\mathrm{cm}^{-3}$. The peak seen on 21 June at around 09:00 UTC (greater than $5\,\mathrm{particles\,cm}^{-3}$) should be attributed to an enhancement in aerosol load, that can be both caused by an intensification of mineral dust burden or ~~, as suggested~~

25   ~~by a~~ by mixing with pollution from the regional PBL (Cristofanelli et al., 2009), as seem to be suggested by the observed corresponding increase in black carbon concentration ~~observed~~ at CMN (see also Cristofanelli et al. (2016))~~, by mixing with pollution from the regional PBL (Cristofanelli et al., 2009)~~. Intermediate depolarization aerosol type 3 is observed below the depolarizing layer, throughout the mineral dust event, and persisting until 22–23 June. As mentioned in the previous section, this can be a signature of mineral dust mixing with local non-depolarizing particulate. ~~The~~ A direct comparison of the aerosol

30   layer structure with the ~~in-situ measurement indicates, in fact,~~ in situ measurement is presented in Fig. 5, focusing on the days of dust transport. From the comparison is possible indeed to observe a simultaneous enhancement of coarse ($2\,\mathrm{\mu m} < Dp < 5\,\mathrm{\mu m}$) particles ~~observed~~ detection by the APSS on 20-22 June (panel ~~b~~ a of Fig. ~~4~~ 5) in correspondence of the identification of type 3 class near the ground, suggesting mineral dust presence in the layer composition. It's worth to notice that, while ground

measurements do not indicate a clear coarse particle enhancement after 22 June, the LiDAR still ~~observed~~ observes a lofted layer of intermediate depolarizing aerosol until 23 June. During the second event (~~28~~ 29 June to 3 July) high wind speeds above 2000 m (up to 20 m s^{-1}) are associated with a ~~high pressure~~ high-pressure area centred above central Italy, leading again to favourable south-westerly circulation. LiDAR data show a second layer of enhanced ~~R ($1 - 1/R$~~ Ra ($Ra/(Ra+1)$ around 0.6) lasting from 28 June at 23:00 UTC to July 3 at 00:00 UTC. Depolarization reaches values higher than in the previous event (with mean values of 15 % and maximum exceeding 20 %); this is again visible as a thick and persistent layer of type 2 aerosol that, in this case, extends down to the ground on 1 July (see panel b of Fig. 5). As in the previous case, it is possible to observe the presence of intermediate depolarization particles (type 3) close to the depolarizing layer (type 2). The dust layer appears to be characterized by a more intense contribution of coarse particles respect to the previous event, visible both at lofted level and ground. ~~In corresponence of the presence of a depolarizing layer at 2000 , the OPC (panel c, Fig. 4) shows coarse particle concentrations nearly doubled compared to the previous event (concentration between 2 and 3). Similarly, in situ observations at SPC (panel b, Fig. 4)~~ APSS observations in fact show an increase in coarse ~~particles~~ particle volume simultaneously to detection of type 2 and 3 particles close to the ground, with values higher than in the previous event (>1 μm^{3}cm^{-3}) and increased contribution from the intermediate ~~particles sizes~~ particle size (1 μm – 2 μm). Similarly, in correspondence of the presence of the depolarizing layer at 2000 m, the OPC (panel c, Fig. 4) shows coarse particle concentrations nearly doubled compared to the previous event (concentration between 2 and 3 particles cm^{-3}).

The upper panels of Fig. 6 shows the footprints of the 5 days retro-plumes released on ~~the~~ 20 June at 18:00 UTC (panel a) and on ~~the~~ 29 June at 12:00 UTC (panel b). The transport for the first event has a more direct pathway, with an average transport time of 2 days from North Sahara. The second event appears instead to originate from Western Sahara and has a longer pathway revolving around the anticyclonic circulation (around 4 days). Aerosol Optical Depth from multi-model forecasts (SDS-WAS Sand and Dust Storm WMO warning advisory and assessment system, visible at http://sds-was.aemet.es/forecast-products/dust-forecasts/compared-dust-forecasts) indicates a spatial distribution in agreement with the FLEXPART footprints for the two events. The simulated mineral dust ~~concentration~~ mass fraction over the SPC site ~~, derived by the coupling of FLEXPART footprint with DREAM emissions~~ (panel c, Fig. 6), allows ~~to provide~~ providing an estimate of the evolution (with a time step of 6 hours) of the mineral dust ~~concentration~~ contribution on the SPC site. The simulation confirms the presence of the two desert dust transport periods and the progressive descent of the dust layers advection from 3000–4000 m to 1000–2000 m heights, simultaneously to what shown by LiDAR observations. ~~Maximum mineral aerosol load~~ The maximum mineral aerosol fraction from FLEXPART analysis occurs on June 20, both at the upper layer (~~12–13~~ 9%) and at the bottom layer (~~11). These concentrations lie in the range of past observations collected over the Northern Mediterranean area (estimated to be around 10 during June–July months)(Pey et al., 2013)~~ 9% also). According to FLEXPART, the import of mineral dust at the lower layer persists until the morning of 23 June, when dust presence is not ~~unambiguosly~~ unambiguously inferable from observations but the aerosol mask still indicates the presence of intermediate depolarizing particles below 2000 m. The second desert dust event predicted by FLEXPART again shows the same timing with respect to ~~observations but, while the APSS and the OPSS indicate a similar dust burden for the two desert aerosol advection events, the dust load indicated by the model (between 3 and 5) appears lower~~ observation and also confirms the presence of a thick layer of dust that involves at the same

time the 1000–2000 m and 3000–4000 m layers. The estimated mass fraction contribution on the contrary, especially in the lower layer (between 2 and 4 %) appears inferior respect to the previous events. It should be emphasized that a quantitative assessment of the mineral aerosol transport ~~is~~ from this method would be difficult, due to uncertainties related to the ~~fixed height of PBL over desert for mineral dust uptake and to~~ model estimate of PBL height over the desert, to the variability in the

5   emissions of mineral dust and to the uncertainties on the ~~emission estimate and on~~ trajectories dynamics (Stohl et al., 1998). ~~Despite~~ Nonetheless, despite such limitations, the model offers a robust characterization of the dynamics and timing of the events, supporting the interpretation of the data analysis.

5   Mean daily variability

Figure 7 reports the frequency of observations for each of the three classes, integrated for the period 15 June – 5 July. Depolar-

10   izing aerosol (panel a, Fig. 7) are associated with the two events of desert dust and hence are mostly observed between 1500 and 5000 m height with a frequency of occurrence ranging between 15 % and 30 %. Non-negligible occurrences ($\sim$ 10 %) are also observed close to the ground and can be attributed to the mineral dust descent during the second event. Non-depolarizing aerosol (panel c, Fig. 7) is dominant throughout the campaign (occurrence up to 80 % below 2000 m); This class of aerosol appears to be mainly confined below the PBL top (derived by the analysis shown in Fig. S1 of the supplementary material and

15   traced with a black dashed line). During the campaign, diurnal PBL starts to develop on average at 06:00 UTC and reaches its maximum vertical extension, up to 2 km height, between 17:00 and 18:00 UTC. ~~An~~ A high occurrence of non-depolarizing particles marks the PBL average daily evolution both during the diurnal formation and at night-time (21:00 to 05:00 UTC), forming the residual layer. A clear minimum of non-depolarizing particles occurrence is observed in the afternoon between 16:00 and 19:00 UTC, when LiDAR indicates instead a maximum (50 % of observation) of intermediate depolarization type occurrence

20   (panel b, Fig. 7). Such enhancement of type 3 particles detection during late afternoon appears frequently along the campaign (clearly visible on 13 days over 21, see Fig. 2). It should be noticed that on 20–22 June and 30 June–2 July the presence of mineral dust can mask any δ_a enhancement in the PBL. On average the vertical extent of such layer of intermediate depolarization is limited within the PBL below 1500 m height (panel b, Fig. 7). ~~The mean diurnal evolution of the different classes, integrated temporally between the four synoptic hours (00:00 UTC, 06:00 UTC, 12:00 UTC, 18:00 UTC) and vertically, below and above~~

25   ~~2000 , is summarized in Fig. ??. Overall, aerosol are mainly observed below 2000 with non-depolarizing aerosol being the predominant type (between 50 and 60 of the observations through the whole day). Intermediate depolarizing type shows its diurnal cycle with an increase in detection from 9 in the early hours to 22 during afternoon and late evening. Desert dust is observed at ground with a non negligible occurrence (7) during the campaign. Aerosol is observed above 2000 in less than 50 of the observations, mainly associated to mineral dust presence (contributing from 13 to 21 of the detections). Average daily~~

30   Daily average evolution of particle volume size distribution~~evolution~~, relatively to ~~dust free~~ dust-free days, is reported in Fig. 8. Fine particles ($Dp < 1 \, \mu m$) volume shows a semidiurnal cycle, corresponding to the diurnal cycle of non-depolarizing aerosol near the ground, with concentration increasing during the stable nocturnal layer phase (late night - early morning) and strongly decreasing during the stage of well-developed PBL. The larger ~~particles~~ particle mode shows two maxima: a first one (volumes

$< 0.4 \ \mu m^3 \ cm^{-3}$), in correspondence to the uplift of the PBL layer around 9:00 UTC, and a second one forming at 15:00 UTC, with a maximum (volumes $> 0.5 \ \mu m^3 \ cm^{-3}$) at 20:00 UTC, showing a similar timing than the depolarization enhancement described above. Further analysis ~~on~~ of the afternoon PBL aerosol composition is reported in the following section.

6   Non desert dust depolarising aerosol

We report in Fig. 9 the δ_a profiles of a representative case study (3 July) of the late afternoon occurrence of intermediate depolarizing aerosol. The aerosol ~~depolarization~~ linear depolarization ratio indicates that the plume starts to develop from 15:00 UTC to 20:00 UTC and reaches the maximum height of 1500 m in the late evening, with a vertical structure suggesting a possible uplift of particles from the ground. An increase in ~~LiDAR aerosol depolarization in~~ aerosol linear depolarization ratio in a regime of convective PBL was already observed by Gibert et al. (2007a). Their results show a positive correlation of enhanced δ_a with an increase in vertical wind velocity, possibly indicating a source emission of particles transported upward by convection. The actual nature of the aerosol plume cannot be assessed solely by LiDAR depolarization. An increase in depolarization can be due to the presence of irregularly shaped particles that can belong to a wide range of aerosol ~~type~~types, from soil and desert dust ~~,~~ to marine aerosol (Murayama et al., 1999) and ash particles (Nisantzi et al., 2014). The hourly time resolution measurements of PM1 and PM10 aerosol chemical compositions, provided by the MARGA analyser, show no evident correlation between the depolarization increase and the presence of sea salt (not reported here). Similarly, no correlation was found with absorbing aerosol (black carbon), investigated by means of a multi-angle absorption photometer (MAAP, Petzold et al., 2006b) (also not shown). By contrast, MARGA observations highlight a maximum in PM10 calcium concentrations, simultaneously to the afternoon increase in ground depolarization (starting between 15:00 and 20:00 UTC, see panel b of Fig. 7) and in the larger particles detection from APSS (maxima between 18:00 and 20:00 UTC, Fig. 8). The diurnal mean evolution of the calcium ion (Ca2+) fraction, calculated over the total PM10 ions, shows a marked increase after 10:00 UTC with a maximum in the late afternoon (17:00 UTC – 20:00 UTC, up to 0.35, see panel a , Fig.10). This daily ~~behavior~~ behaviour is in agreement with the enhancement in aerosol volume contribution from large particles respect to the fine ones, shown in panel b of Fig. 10. These results reinforce the ~~hypotesis~~ hypothesis of the crustal origin of the intermediate depolarizing particles observed by the LiDAR. It is possible therefore to explain, at least on a qualitative basis, the recurrent detection of the afternoon aerosol plumes as emissions and resuspension of soil particles from dried land sources. The frequent occurrence of such events during the observational campaign indicates that the Po Valley can effectively act as a source of mineral particles, likely originated from agricultural soils, that under convective atmospheric conditions can be uplifted at the PBL top in late afternoon hours. This is further confirmed by the diurnal evolution of non-desert dust coarse ~~particles~~ particle concentration at CMN (panel c, Fig. 10), that indicates an enhancement in the coarse ~~particles~~ particle fraction in late afternoon/evening. Hence, recurrent vertical transport from the Po Valley, triggered by thermal air-mass, can uplift mineral aerosol over the mountains ridge, and potentially impact on particulate transport up to the regional scale (Cristofanelli et al., 2016).

7 Effect of aerosol hygroscopic growth on ~~aerosol particles light~~ scattering and depolarization

LiDAR data (Fig. 2) frequently show, during early morning hours, a shallow layer of non-depolarizing aerosol below 300 m height, more easily visible during days characterized by desert dust and mixed dust events (see for instance 00:00-06:00 UTC of ~~the~~ 19 June and between 00:00-08:00 UTC of 30 June). The decrease in depolarization is less evident in dust-free atmosphere but is nevertheless observed in several other days of the campaign (18 June, 21 June, 22 June, 29 June, 1 July, 4 July and 5 July), always below 300 m, before 08:00 UTC and usually associated ~~to~~ with high values of ~~R ($1 - 1/R$~~ Ra ($Ra/(Ra+1)$ > 0.6). ~~A detailed time-height evolution~~ The average profiles of δ_a ~~and~~, relative humidity (RH) ~~for the~~ and potential temperature (TH) for dust-free and dust days at 05:00 UTC (selected among the days of dust presence at the ground: 20–22 June and 30 June ~~(here considered representative of~~ – 2 July) are reported in Fig. 11. During dust-free days (Fig. 11, panel a), values of δ_a stay on average below 1% in the upper layer (above 2000 m) and below 2% in the lower layer (below 2000 m). Starting from 800 m, RH increases with decreasing altitude and this is associated with a progressive decrease in the ~~abovementioned events) is reported in~~ δ_a values. During dust days (Fig. 11, panel b) a more defined stratification of the atmosphere is observed. This is visible also in the profiles of TH that, compared to the dust-free days, shows a clear passage from a stable layer below 500 m to a more unstable one in correspondence of the depolarizing aerosol. The mineral dust plume is ~~clearly visible throughout the depolarization profile. Between 1000~~ visible between 1500 m and 4000 m height, associated with a layer of higher depolarization (δ_a > 10 %) ~~is associated to dry air (~~and drier air respect to the lowermost layer (with RH ~~< 50~~ increasing with height from 40 to 60 %). Below ~~1000~~ 1500 m height, RH varies between ~~50~~ 55 % and ~~70~~ 60 % and δ_a shows lower values compatible with dust presence mixed with local pollution (around ~~4~~ 6 %). Conversely, the lowermost troposphere (below ~~300~~ 500 m), marked by the increased stability shown by the TH profile, is characterized by a ~~layer with a~~ sharp decrease in δ_a (~~less than 2~~ from 7 % down to 3 %) associated ~~to a marked~~ with the increase in RH (~~larger than 80~~ from 50 % to 75 %). The study ~~, extended separatedly on the whole dust events period (20–23 June and 29 June − 2 July, lower panel of Fig. S2, supplementary material) and in the remaining dust free days (upper panel of Fig S2, supplementary material),~~ indicates in both ~~case a depolarization decrease~~ cases a decrease of the depolarization in the lower layers ~~, visible starting from~~ for RH>60%. During ~~dust free~~ dust-free days the affected aerosol layer (below 400 m) shows a depolarization decrease of about 1% (from an average value of 2% to values around 1% and less). During dust days the process influences the aerosol layers at different levels: for RH values between 60% and 65%, depolarization values decrease is around 2% (from more than 7% to around 5.5%). ~~With~~ Closest to the ground, the effect is more evident with increasing RH (~~RH>~~up to ∼70%)~~the effect is more evident,~~, corresponding with a decrease ~~down~~ of depolarization up to 3.5%. This low depolarization near ground suggests the presence of increasingly spherical particles, which can be originated by two different processes:

– the presence of fine particles of anthropogenic origin that may deliquesce: The stagnant meteorological conditions that characterize the Po Valley during anticyclonic phases are ~~favorable~~ favourable for the formation of secondary inorganic aerosols (especially ammonium nitrate) and of secondary organic aerosol (Sandrini et al. , 2016). A recent study (Hodas et al., 2014) showed that, during the same 2012 campaign at SPC, the aerosol liquid water was mainly driven by locally

formed nitrate, hence the growth of spherical non-depolarizing aerosol could occur due to deliquescence of fine particles of anthropogenic origin, of which nitrates were the dominant compound.

- Mechanisms explaining the increase of scattering of mineral dust particles, along with a reduction of their depolarization ratio, can also be hypothesized (Ikegami et al., 1993; Murayama et al., 1999; Sassen et al., 2002; Zhou et al., 2002; Nee et al., 2007). It should be emphasized that, during the analysed case study, high relative humidity values (80 % or more) are observed in the lowermost non-depolarizing layer (see Fig. 11), suggesting that condensation of water around mineral dust particles coated ~~by~~ with (or simply enriched of) hydrophilic components may play a role in the modification of the optical properties of desert dust in this atmospheric layer. Indeed, even if mineral dust is primarily a hydrophobic aerosol, it can become hydrophilic due to chemical reactions occurring on the ~~particles~~ particle surfaces during long-range transport (Nee et al., 2007; Sullivan et al., 2009a) or locally from the condensation of inorganic and organic soluble materials from ground sources.

During the summer 2012 campaign, under the observed conditions, both processes may have played a relevant role: Fig. 12 shows that, during the stagnation phase (from 14 June until 19 June), aerosol nitrate (NO3-) ~~concentrations~~ concentration in both fine and large particles MARGA channels (PM1 and PM10) ~~increase~~ increases with a marked daily cycle peaking at night. The submicron fraction of nitrate dominates the concentration of PM10 nitrate during this phase. The APSS submicron particle volume concentration follows a daily variability and a buildup similar to ~~what~~ that shown by the APSS nitrates ~~concentrations~~concentration, reaching maxima during ~~the~~ 19 June (APSS volume concentration up to 25 μm m^{-3} and NO3-PM1 and PM10 concentration up to 15 μg m^{-3} and 18 μg m^{-3}, respectively). Such increase, evident during early morning hours in small aerosol from APSS and in PM1 nitrate from MARGA, supports the hypothesis of ~~deliquescence of~~ anthropogenic fine particles ~~explaining the low aerosol depolarization~~ deliquescence, explaining therefore the low values of δ_a observed by the LiDAR in the surface layer ~~, particularly~~ during dust-free days. Similarly, ~~under dust presence~~ in presence of dust, the low depolarization values can be related to external mixing of dust depolarizing particles with such locally formed spherical particles. Nevertheless, after the end of the stagnation phase (19 June) the aerosol nitrate concentration decreased and, during the observed desert dust episodes, the difference between the nitrate PM10 and PM1 fractions became more evident, with PM10 prevailing over PM1. The intensified ventilation established after 19 June may in fact have limited the accumulation of anthropogenic particles, at the same time carrying dryer African air masses and making nitric acid condensation on coarse particles ~~prevail~~ prevails over condensation on accumulation mode aerosol. Consequently coarse-mode nitrate would promote water condensation on the large particles, leading to low aerosol ~~depolarization~~ linear depolarization ratio values even in presence of dust.

8 Conclusions

The presented paper provided a characterization of the effects of meteorological evolution and transport patterns on the aerosol variability, based on the observations collected during two major field campaigns (PEGASOS and SuperSito) in the eastern

part of the Po Valley. The aim was to contribute to the understanding of the processes that lead to the high concentration and variability of aerosol characterizing the Po Valley during typical summer conditions.

The analysis of meteorological conditions, coupled with observations from LiDAR and in situ aerosol number/size distribution spectrometers, led to the identification of distinct meteorological regimes with a temporal and spatial distribution of different aerosol types.

We identified a first phase (15–18 June), characterized by a stagnation period (weak winds below 2000 m), representative of hot and polluted conditions in the Po Valley whole area, with progressive accumulation of locally emitted aerosol in the lower troposphere and consequent increase of the fine mode aerosol concentration near the ground. Particle concentration at the ground showed therefore a clear diurnal cycle with maxima during the early morning, when PBL uplift and vertical mixing were absent.

Observations and Lagrangian analysis allowed then a detailed description of two events of Saharan dust transport (in line with the average occurrence of 2–3 summer desert dust episodes over the region detected by satellite (Gkikas et al., 2013)). Mineral dust layers were advected over the measurement site from the Sahara desert, travelling along anticyclonic patterns at high level (around 3000–4000 m) and carrying depolarizing aerosol. The study offered evidence of dust transport to the ground, showing clear dust layers intrusion in the PBL and rapid mixing with local pollution. We showed how this mixed layer, generally characterized by lower depolarization values, can reach the ground within few hours and we showed, by direct comparison with ground in situ instruments, the corresponding enhancement of particle volume size distribution in the 2-5 μm range (leading to values higher than 1 $\mu m^3 cm^{-3}$). In both events the plumes descended indeed to low height (with a total occurrence of depolarizing aerosol identification inside the PBL of $\sim$7 % along the whole campaign). As, on a climatological basis, Saharan dust advection occurs with noticeable frequency over Northern Mediterranean (i.e. Pey et al. (2013) indicated a frequency of 17 % for the 2001–2011 period), dust intrusion can represent a significant factor in increasing PM concentration at the ground. Such results give direct evidence to the suggestion of Bonasoni et al. (2004) that hypothesized, based on in situ measurements in North Italy and back-trajectories analysis, that mineral dust events detected in free troposphere can lead, with non-negligible frequency, to PM10 exceedance at the ground in the time span of some hours.

The study revealed moreover the presence of events of late afternoon particles resuspension from the soil, not related to Saharan dust transport, impacting on the PM concentration near the ground. The existence of a contribution to PM10 levels from resuspension aerosol sources in European regions was already hypothesized by Vautard et al. (2005), based on chemical transport model study. Here, several events of

16

intermediate depolarizing aerosol (mean diurnal frequency of detection ∼22 %), up to 2000 m height, were observed during late afternoon (17:00–20:00) in ~~non-dust~~ dust-free days. The concurrent increase in calcium particle spectroscopic measurements (with a contribution up to 0.35 of the total PM10 fraction) indicated the crustal nature of such aerosol, and can therefore

5 be reasonably attributed to processes of vertical uplift of soil particles, likely related to regional activities (i.e. farming or combustion processes). The vertical extension of such plume, as observed in LiDAR profiles and in the diurnal variability in the CMN measurements, suggests also that local pollution can be transported above mountains peak and ~~therefore~~ hence potentially exported outside the orographic boundaries of the region.

The combination of depolarization profiles with meteorological and aerosol measurements ~~allowed also to identify the presence of a shallow layer of low depolarizing ($\delta_a < 2$) aerosol at the ground, in correspondence to~~ also allowed highlighting

10 the effects of the condition of high RH (typical for this region) on the particle processes. The analysis revealed how, in conditions of high relative humidity values ($RH >$ ~~80~~ 60 %) ~~. The timing~~ in a shallow layer near the ground (<500 m), the aerosol linear depolarization ratio decreases respect to the above atmospheric layer. Such effect is particularly visible when mineral dust particles are present near the ground. During this period, the temporal evolution and the high values of nitrates ~~ions concentration (up to 18)~~ ion concentration in the PM1 and PM10 channels ~~, indicated~~ suggest that the origin of such low

15 depolarization particles can be related to processes of secondary organic aerosol formation and hygroscopic growth on mineral dust particles with a nitrate-enriched surface.

In conclusion, the in-depth analysis of the aerosol light backscattering profiles provided new insights on particles behaviour from the ground up to free troposphere. Results pointed out particles processes, observed relatively frequently on the ~~time span~~ period of the campaign, ~~impacting~~ that impact aerosol variability, air quality and ~~, potentially , regional climateand~~

20 ~~deserving~~ potentially regional climate, and that deserve therefore more extended analysis from longer-period vertical resolved observations (i.e. EARLINET network). The detailed retrieved information (vertical stratification, hygroscopic growth near ground, aerosol evolution inside the PBL) can also ~~serve as a support for~~ support larger scale studies. ~~We cite here as an example~~ As an example, we cite here a recent study, based on MAIAC satellite information (Arvani et al. , 2016), that tries to assess a method for surface PM retrieval from space observations relying on rough approximations of PBL evolution and

25 RH effect on aerosols. Accurate studies on ~~such aspects , as the one proposed here~~ aspects as the ones we presented here may, therefore, ~~can therefore~~ represent an important contribution ~~in~~ to the improvement of more complex and focused atmospheric observation techniques.

17

References

Amiridis, V., Balis, D. S., Kazadzis, S., Bais, A., Giannakaki, E., Papayannis, A., and Zerefos, C.: Four-year aerosol observations with a Raman LiDAR at Thessaloniki, Greece, in the framework of European Aerosol Research LiDAR Network (EARLINET), J. Geophys. Res., 110, D21203, doi:10.1029/2005JD006190, 2005.

5 Amiridis, V., Melas, D., Balis, D. S., Papayannis, A., Founda, D., Katragkou, E., Giannakaki, E., Mamouri, R. E., Gerasopoulos, E., and Zerefos, C.: Aerosol LiDAR observations and model calculations of the Planetary Boundary Layer evolution over Greece during the March 2006 Total Solar Eclipse, Atmos. Chem. Phys., 7, 6181–6189, doi:10.5194/acp-7-6181-2007, 2007.

Andrews, E., Ogren, J. A., Bonasoni, P., Marinoni, A., Cuevas, E., Rodríguez, S., Sun, J. Y., Jaffe, D. A., Fischer, E. V., Baltensperger, U., Weingartner, E., Collaud Coen, M., Sharma, S., Macdonald, A. M., Leaitch, W. R., Lin, N.-H., Laj, P., Arsov, T., Kalapov, 10 I., Jefferson, A., and Sheridan, P.: Climatology of aerosol radiative properties in the free troposphere, Atmos. Res., 102, 365–393, doi:10.1016/j.atmosres.2011.08.017, 2011.

Arvani, B., Pierce,R. B., Lyapustin, A. I., Wang, Y., Ghermandi, G., Teggi, S.: Seasonal monitoring and estimation of regional aerosol distribution over Po valley, northern Italy, using a high–resolution MAIAC product, Atmospheric Environment, Volume 141, 106-121, ISSN 1352-2310, http://dx.doi.org/10.1016/j.atmosenv.2016.06.037, 2016.

15 ~~Basart, S., Prez, C., Nickovic, S., Cuevas, E.~~

Behrendt A. and Nakamura T.: Calculation of the calibration constant of polarization lidar and its dependency on atmospheric temperature, Opt. Express 10, 805-817, ~~Baldasano, J.: Development and evaluation of the BSC-DREAM8b dust regional model over Northern Africa, the Mediterranean and the Middle East. Tellus B, 64. doi:http://dx.doi.org/10.3402/tellusb. v64i0.18539, 2012.~~ 2002

Bonasoni, P., F. Evangelisti, U. Bonafʻe, F. Ravegnani, F. Calzolari, L. Tositti, O. Tubertini, and T. Colombo: Stratospheric ozone 20 intrusion episodes recorded at Mt. Cimone during the VOTALP project: Case studies, Atmos. Environ., 34, 1355–1365, 2000a.

Bonasoni, P., P. Cristofanelli, F. Calzolari, U. Bonafé, F. Evangelisti, A. Stohl, R. van Dingenen, T. Colombo, and Y. Balkanski: Aerosol-ozone correlations during dust transport episodes, Atmos. Chem. Phys., 4, 1201–1215, 2004.

Browell, E. V., C. F. Butler, S. Ismail, P. A. Robinette, A. F. Carter, N. S. Higdon, O. B. Toon, M. R. Schoeberl, and A. F. Tuck: Airborne LiDAR observation in the wintertime arctic stratosphere: Polar stratospheric clouds, Geophys. Res. Lett., 17, 385–388, 1990

25 Burton, S. P., Ferrare, R. A., Hostetler, C. A., Hair, J. W., Rogers, R. R., Obland, M. D., Butler, C. F., Cook, A. L., Harper, D. B., and Froyd, K. D.: Aerosol classification using airborne High Spectral Resolution LiDAR measurements – methodology and examples, Atmos. Meas. Tech., 5, 73-98, doi:10.5194/amt-5-73-2012, 2012.

Cairo, F., Di Donfrancesco, G., Adriani, A., Pulvirenti, L., and Fierli, F.: Comparison of Various Linear Depolarization Parameters Measured by LiDAR, Appl. Optics, 38, 4425–4432, 1999.

30 Cairo, F., G.. Di Donfrancesco, L.. Di Liberto, and M.. Viterbini: The RAMNI airborne LiDAR for cloud and aerosol research, Atmos. Meas. Tech., vol. 5, no. 7, pp. 1779-1792, 2012.

Carnevale, C., G. Finzi, E. Pisoni, M. Volta, P. Kishcha, P. Alpert, Integrating Saharan dust forecasts into a regional chemical transport model: A case study over Northern Italy, Science of The Total Environment, Volumes 417–418, 224-231, ISSN 0048-9697, http://dx.doi.org/10.1016/j.scitotenv.2011.12.031, 2012.

35 Chen, W. N., Chiang, C. W., and Nee, J. B.: LiDAR ratio and depolarization ratio for cirrus clouds, Appl. Opt., 41, 6470-6476, 2002.

Clarisse, L., Clerbaux, C., Dentener, F., Hurtmans, D, Coheur, P.-F.: Global ammonia distribution derived from infrared satellite observations, Nature Geosci. 2, 479 - 483, Published online: 21 June 2009, doi:10.1038/ngeo551, 2009.

Cristofanelli, P., Marinoni, A., Arduini, J., Bonafè, U., Calzolari, F., Colombo, T., Decesari, S., Duchi, R., Facchini, M. C., Fierli, F., Finessi, E., Maione, M., Chiari, M., Calzolai, G., Messina, P., Orlandi, E., Roccato, F., and Bonasoni, P.: Significant variations of trace gas composition and aerosol properties at Mt. Cimone during air mass transport from North Africa - contributions from wildfire emissions and mineral dust, Atmos. Chem. Phys., 9, 4603-4619, doi:10.5194/acp-9-4603-2009, 2009.

5 Cristofanelli, P., Fierli, F., Marinoni, A., Calzolari, F., Duchi, R., Burkhart, J., Stohl, A., Maione, M., Arduini, J., and Bonasoni, P.: Influence of biomass burning and anthropogenic emissions on ozone, carbon monoxide and black carbon at the Mt. Cimone GAW-WMO global station (Italy, 2165 m a.s.l.), Atmos. Chem. Phys., 13, 15-30, doi:10.5194/acp-13-15-2013, 2013.

Cristofanelli, P., Landi, T.C., Calzolari, F., Duchi, R., Marinoni, A., Rinaldi, M., Bonasoni, P.: Summer atmospheric composition over the Mediterranean basin: Investigation on transport processes and pollutant export to the free troposphere by observations at the WMO/GAW
10 Mt. Cimone global station (Italy, 2165 m a.s.l.), Atm. Env., 141, 139-152, ISSN 1352-2310, doi:10.1016/j.atmosenv.2016.06.048., 2016.

Crosier, J., Allan, J. D., Coe, H., Bower, K. N., Formenti, P., and Williams, P. I.: Chemical composition of summertime aerosol in the Po Valley (Italy), northern Adriatic and Black Sea, Q. J. R. Meteorol. Soc., 133, 61-75, 10.1002/qj.88, 2007.

Decesari, S., Allan, J., Plass-Duelmer, C., Williams, B. J., Paglione, M., Facchini, M. C., O'Dowd, C., Harrison, R. M., Gietl, J. K., Coe, H., Giulianelli, L., Gobbi, G. P., Lanconelli, C., Carbone, C., Worsnop, D., Lambe, A. T., Ahern, A. T., Moretti, F., Tagliavini, E., Elste,
15 T., Gilge, S., Zhang, Y., and Dall'Osto, M.: Measurements of the aerosol chemical composition and mixing state in the Po Valley using multiple spectroscopic techniques, Atmos. Chem. Phys., 14, 12109-12132, doi:10.5194/acp-14-12109-2014, 2014.

Duchi R, Cristofanelli P, Landi TC, Arduini J, Bonafé U, Bourcier, L., Busetto, M., Calzolari, F., Marinoni, A., Putero, D., Bonasoni, P.: Long-term (2002–2012) investigation of Saharan dust transport events at Mt. Cimone GAW global station, Italy (2165 m a.s.l.). Elem Sci Anth 4: 000085. doi: 10.12952/journal.elementa.000085, 2016.

20 Dulac, F., and P. Chazette: Airborne study of a multi-layer aerosol structure in the eastern Mediterranean observed with the airborne polarized LiDAR ALEX during a STAAARTE campaign (7 June 1997), Atmos. Chem. Phys., 3, 1817–1831, 2003.

Eloranta, E. W., I. A. Razenkov, and J. P. Garcia: Mixed-phase cloud measurements with the University of Wisconsin high spectral resolution LiDAR, paper presented at 16th Science Team Meeting, Atmos. Radiat. Meas., Albuquerque, N. M., 27–31 March, 2006.

Escudero, M., S. Castillo, X. Querol, A. Avila, M. Alarcón, M. M. Viana, A. Alastuey, E. Cuevas, and S. Rodríguez: Wet and dry African
25 dust episodes over Eastern Spain, J. Geophys. Res., 110, D18S08, doi:10.1029/2004JD004731,2005.

Flamant C, Chaboureau J-P, Parker DP, Taylor CM, Cammas JP, Bock O, Timouk F, Pelon J.: Airborne observations of the impact of a convective system on the planetary boundary-layer thermodynamics and aerosol distribution in the intertropical discontinuity region of the West African Monsoon. Q. J. R. Meteorol. Soc. 133: 1175-1189, 2007.

Fernald, F. G.: Analysis of atmospheric LiDAR observations: some comments, Appl. Optics, 23, 652-653, 1984.

30 Ferrare R. A., D. D. Turner, L. Heilman Brasseur, W. F. Feltz, O. Dubovik, and T. P. Tooman: Raman LiDAR measurements of the aerosol extinction-to-backscatter ratio over the Southern Great Plains, J. of Geophys. Res.,106,20333-20347, 2001.

Fiebig, M., Petzold, A., Wandinger, U., Wendisch, W., Kiemle, C., Stifter, A., Ebert, M., Rother, T., and Leiterer, U.: Method, accuracy, and inferable properties applied to a biomass-burning aerosol and its radiative forcing, J. Geophys. Res., 107, 8130, doi:10.1029/2000JD000192, 2002.

35 Flentje, H., Heese, B., Reichardt, J., and Thomas, W.: Aerosol profiling using the ceilometer network of the German Meteorological Service, Atmos. Meas. Tech. Discuss., 3, 3643-3673, doi:10.5194/amtd-3-3643-2010, 2010.

Forster, P., Ramaswamy, V., Artaxo, P., Berntsen, T., Betts, R., Fahey, D. W., Haywood, J., Lean, J., Lowe, D. C., Myhre, G., Nganga, J., Prinn, R., Raga, G., Schulz, M., and Van Dorland, R.: Radiative Forcing of Climate Change, in Climate Change 2007: The Physical

Science Basis. Contribution of Working Group I to the Fourth Assessment Report of the Intergovernmental Panel on Climate Change, edited by S. Solomon, D. Qin, M. Manning, Z. Chen, M. Marquis, K. B. Averyt, M. Tignor, and H. L. Miller, pp. 129-234, Cambridge Univ. Press, Cambridge, United Kingdom and New York, NY, USA, 2007.

Freudenthaler, V., Esselborn, M., Wiegner, M., Heese, B., Tesche, M., Ansmann, A., Muller, D., Althausen, D., Wirth, M., Fix, A.,Ëhret, G., Knippertz, P., Toledano, C., Gasteiger, J., Garhammer, M., and Seefeldner, M.: Depolarization ratio profiling at several wavelengths in pure Saharan dust during SAMUM 2006, Tellus B, 61, 165-179, doi:10.1111/j.1600-0889.2008.00396.x, 2009.

Freudenthaler, V.: About the effects of polarising optics on lidar signals and the ?90 calibration, Atmos. Meas. Tech., 9, 4181-4255, https://doi.org/10.5194/amt-9-4181-2016, 2016

Gibert, F. , J. Cuesta, J.-I. Yano, N. Arnault, and P. H. Flamant: On the correlation between convective plume updrafts and downdrafts, LiDAR reflectivity and depolarization ratio. Bound.- Layer Meteor., 125, 553-573, 2007a.

Gkikas A, Hatzianastassiou N, Mihalopoulos N, Katsoulis V, Kazadzis S, Pey J, Querol X, Torres O.: The regime of intense desert dust episodes in the Mediterranean based on contemporary satellite observations and ground measurements. Atmospheric Chemistry and Physics 13: 12135-12154, doi: 10.5194/acp-13-12135-2013, 2013.

Gobbi, G.P., Barnaba, F., Ammannato, L., Estimating the impact of Saharan dust on the year 2001 PM10 record of Rome, Italy. Atmospheric Environment 41 (2),261-275., 2007.

Größ, S., Esselborn, M., Weinzierl, B., Wirth, M., Fix, A., and Petzold, A.: Aerosol classification by airborne high spectral resolution LiDAR observations, Atmos. Chem. Phys., 13, 2487-2505, doi:10.5194/acp-13-2487-2013, 2013.

Hamonou, E., P. Chazette, D. Balis, F. Dulac, X. Schneider, E. Galani, G. Ancellet, and A. Papayannis: Characterization of the vertical structure of Saharan dust export to the Mediterranean basin, J. Geophys. Res., 104, 22,257 - 22,270, 1999.

Hanke, M., B. Umann, J. Uecker, F. Arnold, and H. Bunz: Atmospheric measurements of gas-phase HNO3 and SO2 using chemical ionization mass spectrometry during the MINATROC field campaign 2000 on Monte Cimone, Atmos. Chem. Phys., 3, 417 - 436, 2003.

Hodas, N., Meng, Q.Y., Lunden, M.M., Turpin, B.J.: Toward refined estimates of ambient PM2.5 exposure: Evaluation of a physical outdoor-to-indoor transport model. Atmospheric Environment 83, 229-236, 2014.

Hooper, W. P. and Eloranta, E. W.: LiDAR Measurements of Wind in the Planetary Boundary Layer: the Method, Accuracy and Results from Joint Measurements with Radiosonde and Kytoon, J. Clim. Appl. Meteorol., 25, 990-1001, 1986.

Ikegami,M., Okada,K., Zaizen, Y., Makino,Y.: Aerosol particles in the middle troposphere over the northern Pacific. Journal of the Meteorological Society of Japan 71,517-528, 1993.

Israelevich, P., Ganor, E., Alpert, P., Kishcha, P., and Stupp, A.: Predominant transport paths of Saharan dust over the Mediterranean Sea to Europe, J. Geophys. Res., 117, D02205, doi:10.1029/2011JD016482, 2012.

Jordan, N. S., Hoff, R. M., and Bacmeister, J. T.: Validation of Goddard Earth Observing System-version 5 MERRA Planetary Boundary Layer Heights using CALIPSO, J. Geophys. Res., 115, D24218, doi:10.1029/2009JD013777, 2010.

Kalivitis, N., Gerasopoulos, E., Vrekoussis, M., Kouvarakis, G., Kubilay, N., Hatzianastassiou, N., Vardavas, I., and Mihalopoulos, N.: Dust transport over the eastern Mediterranean derived from Total Ozone Mapping Spectrometer, Aerosol Robotic Network, and surface measurements, J. Geophys. Res.-Atmos., 112, D03202, doi:10.1029/2006JD007510, 2007.

Kanakidou, M., Mihalopoulos, N., Kindap, T., Im, U., Vrekoussis, M., Gerasopoulos, E., Dermitzaki, E., Unal, A., Kocak, M., Markakis, K., Melas, D., Kouvarakis, G., Youssef, A. F., Richter, A., Hatzianastassiou, N., Hilboll, A., Ebojie, F., von Savigny, C., Ladstaetter-Weissenmayer, A., Burrows, J., and Moubasher, H.: Megacities as hot spots of air pollution in the East Mediterranean. Atmos. Environ., 45, 1223–1235, 2011.

Keuken, M. P., Schoonebeek, C. A. M., Vanwensveenlouter, A., and Slanina, J.: Simultaneous Sampling of NH3, HNO3, HCl, SO2 and H2O2 in Ambient Air by a Wet Annular Denuder System, Atmos. Environ., 22, 11, 2541-2548, 1988.

Klett, J. D.: LiDAR inversion with variable backscatter/extinction ratios, Appl. Optics, 24, 1638-1643, 1985.

Khlystov, A., Wyers, G. P., and Slanina, J.: The steam-jet aerosol collector, Atmos. Environ., 29, 2229-2234, 1995.

5 Khlystov, A., Stanier, C., and Pandis S. N.: An algorithm for combining electrical mobility and aerodynamic size distributions data when measuring ambient aerosol, Aeros.Sci. Technol., 38, 229-238, 2004.

Lammert, A. and Bösenberg, J.: Determination of the Convective Boundary Layer Height with Laser Remote Sensing, Bound.- Lay. Meteorol., 119, 159-170, 2006.

Lelieveld, J., Berresheim, H., Borrmann, S., et al.: Global air pollution crossroads over the Mediterranean, Science, 298, 794-799, 2002.

10 Liu, Z. Y., Omar, A., Vaughan, M., Hair, J., Kittaka, C., Hu, Y. X., Powell, K., Trepte, C., Winker, D., Hostetler, C., Ferrare, R., and Pierce, R.: CALIPSO LiDAR observations of the optical properties of Saharan dust: A case study of long-range transport, J. Geophys. Res.-Atmos., 113, D07207, doi:10.1029/2007jd008878, 2008.

Makkonen, U., Virkkula, A., Mäntykenttä, J., Hakola, H., Keronen, P., Vakkari, V., and Aalto, P. P.: Semi-continuous gas and inorganic aerosol measurements at a Finnish urban site: comparisons with filters, nitrogen in aerosol and gas phases, and aerosol acidity, Atmos.
15 Chem. Phys., 12, 5617-5631, doi:10.5194/acp-12-5617-2012, 2012.

Marinoni, A., P. Cristofanelli, F. Calzolari, F. Roccato, U. Bonafé, and P. Bonasoni: Continuous measurements of aerosol physical parameters at the Mt. Cimone GAW Station (2165 m asl, Italy), Science of the Total Environment, vol. 391, no. 2-3, pp. 241-251, 2008.

Martucci, G., Matthey, R., Mitev, V., and Richner, H.: Comparison between Backscatter LiDAR and Radiosonde Measurements of the Diurnal and Nocturnal Stratification in the Lower Troposphere, J. Atmos. Ocean. Technol., 24, 1231-1244, 2007.

20 Matassoni L, Pratesi G, Centioli D, Cadoni F, Malesani P, Caricchia AM, Di Menno di Bucchianico, A.: Saharan dust episodes in Italy: influence on PM10 daily limit value (DLV) exceedances and the related synoptic. J Environ Monit 11:1586-1594., 2009.

Matthias,V., Bockmann, C., Freudenthaler, V., Pappalardo, G., Bösenberg, J., Amiridis, V., Amodeo, A., Ansmann, A., Balis, D. , Boselli, A. ,Chaykovski, A., Chourdakis, G., Comeron, A., Delaval, A., De Tomasi, F., Eixmann, R., Frioud, M., Hagard, A., Iarlori, M. , Komguem, L., Kreipl, S., Larcheveque, G., Linne, H., Matthey, R., Mattis, I., Papayannis, A., Pelon, J., Perrone, R. M. , Persson, R., Resendes, D. P.,
25 Rizi, V., Rocadenbosch, F., Rodriguez, J. A., Sauvage, L., Schneider, J., Schumacher, R., Shcherbakov, V., Simeonov, V., Wandinger, U., Wang, X., Wiegner, M., and Zerefos, C.,: LiDAR intercomparison on algorithm and system level in the frame of EARLINET, MPI Rep. 337, Max-Planck-Inst. f ür Meteorol., Hamburg, Germany, 2002.

Melfi, S. H., J. D. Spinhirne, S.-H. Chou, and S. P. Palm, LiDAR observations of vertically organized convection in the planetary boundary layer over the ocean, J. Clim. Appl. Meteorol., 24, 806 - 821, 1985.

30 Monks, P., Granier, C., Fuzzi, S., Stohl, A., Williams, M., Akimoto, H., Amann, M., Baklanov, A., Baltensperger, U., Bey, I., Blake, N., Blake, R., Carslaw, K., Cooper, O., Dentener, F., Fowler, D., Fragkou, E., Frost, G., Generoso, S., Ginoux, P., Grewe, V., Guen- 25 ther, A., Hansson, H., Henne, S., Hjorth, J., Hofzumahaus, A., Huntrieser, H., Isaksen, I., Jenkin, M., Kaiser, J., Kanakidou, M., Klimont, Z., Kulmala, M., Laj, P., Lawrence, M., Lee, J., Liousse, C., Maione, M., McFiggans, G., Metzger, A., Mieville, A., Moussiopoulos, N., Orlando, J., O'Dowd, C., Palmer, P., Parrish, D., Petzold, A., Platt, U., Pschl, U., Prvt, A., Reeves, C., Reimann, S., Rudich, Y., Sellegri, K., Stein-
35 brecher, R., Simpson, D., 30 ten Brink, H., Theloke, J., van der Werf, G., Vautard, R., Vestreng, V., Vlachokostas, C., and von Glasow, R.: Atmospheric composition change - global and regional air quality, Atmos. Environ., 43, 5268-5350, doi:10.1016/j.atmosenv.2009.08.021, 2009.

Müller, D., Ansmann, A., Mattis, I., Tesche, M., Wandinger, U., Althausen, D., and Pisani, G.: Aerosol-type-dependent LiDAR ratios observed with Raman LiDAR, J. Geophys. Res., 112, doi:10.1029/2006JD008292, 2007.

Müller, D., Mattis, I., Tatarov, B., Noh, Y., Shin, D., Shin, S., Lee, K., Kim, Y., and Sugimoto, N.: Mineral quartz concentration measurements of mixed mineral dust/urban haze pollution plumes over Korea with multiwavelength aerosol Raman-quartz LiDAR, Geophys. Res. Lett., 37, L20810, doi:10.1029/2010GL044633, 2010.

Murayama, T., H. O. N. Kaneyasu, H. Kamataki, and K. Miura, Application of LiDAR depolarization measurement in the atmospheric boundary layer: Effects of dust and sea-salt particles, J. Geophys. Res., 104, 31781 - 31792.,1999.

Murayama, T., Masonis, S. J., Redemann, J., Anderson, T. L., Schmid, B., Livingston, J. M., Russell, P. B., Huebert, B., Howell, S. G., McNaughton, C. S., Clarke, A., Abo, M., Shimizu, A., Sugimoto, N., Yabuki, M., Kuze, H., Fukagawa, S., Maxwell-Meier, K., Weber, R. J., Orsini, D. A., Blomquist, B., Bandy, A., and Thornton, D.: An intercomparison of LiDARderived aerosol optical properties with airborne measurements near Tokyo during ACE-Asia, J. Geophys. Res.-Atmos., 108, 8651, doi:10.1029/2002jd003259, 2003.

Nee, J. B., Chiang, C.-W., Hu, H.-l., Hu, S.-X., and Yu, J.-Y.: LiDAR measurements of Asian dust storms and dust cloud interactions, J. Geophys. Res., 112, D15202, doi:10.1029/2007JD008476, 2007.

Nisantzi, A., Mamouri, R. E., Ansmann, A., and Hadjimitsis, D.: Injection of mineral dust into the free troposphere during fire events observed with polarization LiDAR at Limassol, Cyprus, Atmos. Chem. Phys., 14, 12155-12165, doi:10.5194/acp-14-12155-2014, 2014.

O'Connor, E. J., Illingworth,A. J., and Hogan, R. J., 2004: A technique for autocalibration of cloud LiDAR and for inferring the LiDAR ratio for ice and mixed phase clouds. J. Atmos. Ocean. Technol., 21(5), 777-786, 2004.

Omar, A. H., Winker, D. M., Kittaka, C., Vaughan, M. A., Liu, Z. Y., Hu, Y. X., Trepte, C. R., Rogers, R. R., Ferrare, R. A., Lee, K. P., Kuehn, R. E., and Hostetler, C. A.: The CALIPSO Automated Aerosol Classification and LiDAR Ratio Selection Algorithm, J. Atmos. Ocean. Tech., 26, 1994-2014, doi:10.1175/2009jtecha1231.1, 2009.

Papayannis, A., Balis, D., Amiridis, V., Chourdakis, G., Tsaknakis, G., Zerefos, C., Castanho, A. D. A., Nickovic, S., Kazadzis, S., and Grabowski, J.: Measurements of Saharan dust aerosols over the Eastern Mediterranean using elastic backscatter-Raman LiDAR, spectrophotometric and satellite observations in the frame of the EARLINET project, Atmos. Chem. Phys., 5, 2065-2079,doi:10.5194/acp-5-2065-2005, 2005.

Pappalardo G., A. Amodeo, M. Pandolfi, U. Wandinger, A. Ansmann, J. Bosenberg, V. Matthias, V. Amiridis, F. De Tomasi, M. Frioud, M. Iarlori, L. Komguem, A. Papayannis, F. Rocadenbosch, X. Wang: Aerosol LiDAR intercomparison in the framework of the EARLINET project. 3. Raman LiDAR algorithm for aerosol extinction, backscatter and LiDAR ratio, Appl. Opt., 43. N. 28, 53705385, 2004.

Pavese, G., Calvello, M., Esposito, F., Leone, L., and Restieri, R.: Effects of Saharan dust advection on atmospheric aerosol properties in the West-Mediterranean area, Adv. Meteorol., 2012, 730579, doi:10.1155/2012/730579, 2012.

Pederzoli A, Mircea M, Finardi S, Di Sarra A, Zanini G.: Quantification of Saharan dust contribution to PM10 concentrations over Italy during 2003-2005. Atmos Environ;44:4181-90, 2010.

Prez, C., Nickovic, S., Pejanovic, G., Baldasano, J. M. and Ozsoy, E.: Interactive dust-radiation modeling: a step to improve weather forecasts. J. Geophys. Res. 11, D16206., 2006a.

Prez, C., Nickovic, S., Baldasano, J. M., Sicard, M., Rocadenbosch, F. and Cachorro, V. E. : A long Saharan dust event over the western Mediterranean: LiDAR, Sun photometer observations, and regional dust modeling. J. Geophys. Res. 111, D15214., doi:10.1029/2005JD006579, 2006b.

Perrino, C., Catrambrone, M., Pietrodangelo, A.: Influence of atmospheric stability on the mass concentration and chemical composition of atmospheric particles: a case study in Rome, Italy. Environment International 34, 621-628, 2008.

Petzold, A. and Schonlinner, M.: Multi-Angle Absorption Photometry - A New Method for the Measurement of Aerosol Light Absorption and Atmospheric Black Carbon, J. Aerosol Sci., 35, 421-441, 2004.

Pey, J., Querol, X., Alastuey, A., Forastiere, F., and Stafoggia, M.: African dust outbreaks over the Mediterranean Basin during 2001-2011: PM10 concentrations, phenomenology and trends, and its relation with synoptic and mesoscale meteorology, Atmos. Chem. Phys., 13, 1395-1410, doi:10.5194/acp-13-1395-2013, 2013.

Prospero, J. M., P. Ginoux, O. Torres, S. Nicholson, and T. Gill: Environmental characterization of global sources of atmospheric soil dust identified with the NIMBUS7 Total Ozone Mapping Spectrometer (TOMS) absorbing aerosol product, Rev. Geophys., 40(1), 1002, doi:10.1029/2000RG000095, 2002.

Putaud, J.P., Van Dingenen, R., Dell'Acqua, A., Raes, F., Matta, E., Decesari, S., Facchini, M.C., Fuzzi, S.: Sizesegregated aerosol mass closure and chemical composition in Monte Cimone (I) during MINATROC. Atmospheric Chemistry and Physics 4, 889 - 902, 2004.

Querol, X., Pey, J., Pandolfi, M., Alastuey, A., Cusack, M., Moreno, T., Viana, M., Mihalopoulos, N., Kallos, G., and Kleanthous, S.: African dust contributions to mean ambient PM10 levels across the Mediterranean Basin, Atmos. Environ., 43, 4266- 4277, 2009a.

Rosati, B., Herrmann, E., Bucci, S., Fierli, F., Cairo, F., Gysel, M., Tillmann, R., Größ, J., Gobbi, G. P., Di Liberto, L., Di Donfrancesco, G., Wiedensohler, A., Weingartner, E., Virtanen, A., Mentel, T. F., and Baltensperger, U.: Studying the vertical aerosol extinction coefficient by comparing in situ airborne data and elastic backscatter LiDAR, Atmos. Chem. Phys., 16, 4539-4554, doi:10.5194/acp-16-4539-2016, 2016.

Rossa A., Ferrario M.E., Sansone M., Monai M.: Climatology of the static stability of the night-time Po Valley pbl from radio sondes and passive microwave radiometers. In Proceedings of the 9th International Symposium on Tropospheric Profiling, Cimini D, Di Girolamo P, Marzano FS, Rizi V (eds), L'Aquila, Italy. ESAConference Bureau: Noordwijk, The Netherlands, 2012.

Rumsey, I. C., Cowen, K. A., Walker, J. T., Kelly, T. J., Hanft, E. A., Mishoe, K., Rogers, C., Proost, R., Beachley, G. M., Lear, G., Frelink, T., and Otjes, R. P.: An assessment of the performance of the Monitor for AeRosols and GAses in ambient air (MARGA): a semi-continuous method for soluble compounds, Atmos. Chem. Phys., 14, 5639-5658, doi:10.5194/acp-14-5639-2014, 2014.

Saarikoski, S., Carbone, S., Decesari, S., Giulianelli, L., Angelini, F., Canagaratna, M., Ng, N. L., Trimborn, A., Facchini, M. C., Fuzzi, S., Hillamo, R., and Worsnop, D.: Chemical characterization of springtime submicrometer aerosol in Po Valley, Italy, Atmos. Chem. Phys., 12, 8401-8421, doi:10.5194/acp-12-8401-2012, 2012.

Saha, S., Moorthi, S., Wu, X., Wang, J., Nadiga, S., Tripp, P., Behringer, D., Hou, Y., Chuang, H., Iredell, M., Ek, M., Meng, J., Yang, R., Mendez, M. P., van den Dool, H., Zhang, Q., Wang, W., Chen, M., and Becker, E. (2011): NCEP Climate Forecast System Version 2 (CFSv2) 6-hourly Products. Research Data Archive at the National Center for Atmospheric Research, Computational and Information Systems Laboratory. http://dx.doi.org/10.5065/D61C1TXF, 2011.

Sandrini, S., van Pinxteren, D., Giulianelli, L., Herrmann, H., Poulain, L., Facchini, M. C., Gilardoni, S., Rinaldi, M., Paglione, M., Turpin, B. J., Pollini, F., Zanca, N., and Decesari, S.: Size-resolved aerosol composition at an urban and a rural site in the Po Valley in summertime: implications for secondary aerosol formation, Atmos. Chem. Phys. Discuss., doi:10.5194/acp-2015-1036, in press, 2016.

Salvador, P., S. Alonso-Pérez, J. Pey, B. Artíñano , J. J. de Bustos, A. Alastuey, and X. Querol, African dust outbreaks over the western Mediterranean Basin: 11-year characterization of atmospheric circulation patterns and dust source areas., 2014.

Zauli Sajani, S., Miglio, R., Bonasoni, P., Cristofanelli, P., Marinoni, A., Sartini, C., Goldoni, C. A., De Girolamo, G., and Lauriola, P.: Saharan dust and daily mortality in Emilia-Romagna (Italy), Occupational and Environmental Medicine, 68, 446–451, doi:10.1136/oem.2010.058156, 2011.

Sakai, T., T. Shibata, S.-A. Kwon, Y.-S. Kim, K. Tamura, and Y. Iwasaka: Free tropospheric backscatter, depolarization ratio, and relative humidity measured with the Raman LiDAR at Nagoya in 1994 - 1997: Contributions of aerosols from the Asian continent and the Pacific Ocean, Atmos. Environ., 34, 431 - 442, 2000.

Sassen, K.: Polarization LiDAR evidence at FARS for indirect climate forcing from asian dust stroms, LiDAR remote sensing in atmospheric and earth sciences 21th conference, 483-484., 2002.

Seibert P.,Beyrich, F.,Gryning, S.E.,Joffre, S.,Rasmussen, S., and Tercier, P.: Review and Intercomparison of Operational Methods for the Determination of the Mixing Height. Atmospheric Environment 34(7):1001-1027, 2000.

Shi, A.,Zhang, D., Hayashi, M., Ogata, H., Ji, H., Fujiie, W.: Influences of sulfate and nitrate on the hygroscopic behaviour of coarse dust particles, Atmos. Env., Volume 42, Issue 4, February 2008, Pages 822-827, ISSN 1352-2310, http://dx.doi.org/10.1016/j.atmosenv.2007.10.037, 2008.

Shimizu, A., Sugimoto, N., Matsui, I., Arao, K., Uno, I., Murayama, T., Kagawa, N., Aoki, K., Uchiyama, A., and Yamazaki, A.: Continuous observations of Asian dust and other aerosols by polarization LiDARs in China and Japan during ACE-Asia, J. Geophys. Res., 109, D19S17, doi:10.1029/2002jd003253, 2004.

Sicard, M., C. Pérez, F. Rocadenbosch, J. M. Baldasano, D. García-Vizcaino: Mixed-Layer Depth Determination in the Barcelona Coastal Area From Regular LiDAR Measurements: Methods, Results and Limitations. Bound.Layer Meteor. 119, 135-157, 2006.

Slanina, J., ten Brink, H. M., Otjes, R. P., Even, A., Jongejan, P., Khlystov, A., Waijers-Ijpelaan, A., and Hu, M.: The continuous analysis of nitrate and ammonium in aerosols by the steam jet aerosol collector (SJAC): extension and validation of the methodology, Atmos. Environ., 35, 2319-2330, 2001.

Sorensen,J.H., Rasmussen,A.,Ellermann,T. and Lyck,E.: Mesoscale Influence on Long-range Transport Evidence From ETEX Modeling and Observations, Atmos. Envir., 32(24): 4207-4217, 1998.

Stohl, A.: Computation, accuracy and applications of trajectories - a review and bibliography. Atmos. Environ., 32, 947-966, 1998.

Stohl, A., Forster, C., Frank, A., Seibert, P., Wotawa, G.: Technical note: The Lagrangian particle dispersion model FLEXPART version 6.2., Atmos. Chem. Phys., 5, 2461-2474, 2005.

Stohl, A., Sodemann, H., Eckhardt, S., Frank, A., Seibert, P., Wotawa, G., Morton, D., Arnold, D. and Harustak, M.: The Lagrangian particle dispersion model FLEXPART version 9.3, Tech. rep., Norwegian Institute of Air Research (NILU), Kjeller, Norway, available at: http://flexpart.eu, last access: 2 June 2016, 2010.

Stull, R. B., An Introduction to Boundary Layer Meteorology, Kluwer Acad., Dordrecht, Netherlands,1988.

Sullivan, R. C., M. Moore, M. D. Petters, S. M. Kreidenweis, G. Roberts, and K. A. Prather, Timescale for hygroscopic conversion of mineral dust particles after heterogeneous reaction with nitric acid, Phys. Chem. Chem. Phys., 11, 7826-7837, doi:10.1039/b904217b, 2009a.

Sun, W., Liu, z., Videen, G., Fu, Q.,Muinonen,K., Winker, D.M., Lukashin, C., Jin, Z., Lin, B., Huang, J.: For the depolarization of linearly polarized light by smoke particles, J. Quant. Spectrosc. Radiat. Transfer, 122, 233-237, doi:10.1016/j.jqsrt.2012.03.031.,2012.

Sugimoto, N. and Lee, C. H.: Characteristics of dust aerosols inferred from LiDAR depolarization measurements at two wavelengths, Appl. Optics, 45, 7468-7474, 2006.

Tesche, M., Ansmann, A., Muller, D., Althausen, D., Engelmann, R., Freudenthaler, V., and Groß, S.: Vertically resolved separation of dust and smoke over Cape Verde using multiwavelength Raman and polarization LiDARs during Saharan Mineral Dust Experiment 2008, J. Geophys. Res., 114, D13202, doi:10.1029/2009jd011862, 2009a.

Twigg, M. M., Di Marco, C. F., Leeson, S., van Dijk, N., Jones, M. R., Leith, I. D., Morrison, E., Coyle, M., Proost, R., Peeters, A. N. M., Lemon, E., Frelink, T., Braban, C. F., Nemitz, E., and Cape, J. N.: Water soluble aerosols and gases at a UK background site - Part 1: Controls of PM2.5 and PM10 aerosol composition, Atmos. Chem. Phys., 15, 8131-8145, doi:10.5194/acp-15-8131-2015, 2015.

Van Dingenen, R., Raes, F., Putaud, J. P., Baltensperger, U., Charron, A., Facchini, M. C., Decesari, S., Fuzzi, S., Gehrig, R., Hansson, H. C., Harrison, R. M., Hüglin, C., Jones, A. M., Laj, P.,Lorbeer, G., Maenhaut, W., Palmgren, F., Querol, X., Rodriguez, S., Schneider, J., ten Brink, H., Tunved, P., Tørseth, K., Wehner, B., Weingartner, E., Wiedensohler, A., and Wåhlin, P. A.: European aerosol phenomenology-1: physical characteristics of particulate matter at kerbside, urban, rural and background sites in Europe, Atmos. Environ., 38, 2561-2577, 2004.

Vautard, R., Bessagnet, B., Chin, M., and Menut, L.: On the contribution of natural Aeolian sources to particulate matter concentrations in Europe: Testing hypotheses with a modelling approach, Atmos. Environ., 39(18), 3291-3303, 2005.

Washington, R., Todd, M., Middleton, N. J. and Goudie, A. S.: Dust-Storm Source Areas Determined by the Total Ozone Monitoring Spectrometer and Surface Observations. Annals of the Association of American Geographers, 93: 297-313. doi: 10.1111/1467-8306.9302003 [http://onlinelibrary.wiley.com/doi/10.1111/1467-8306.9302003/epdf], 2003.

Zhou, J., Yu, G., Jin, C., Qi, F., Liu, D., Liu, H., Hu, H., Gong, Z., Shi, G., Nakajima, T., and Takamura, T.,: LiDAR observations of Asian dust over Hefei, China in spring 2000, J. Geophys. Res., 107(D), 4252, doi:10.1029/2001JD000802, 2002.
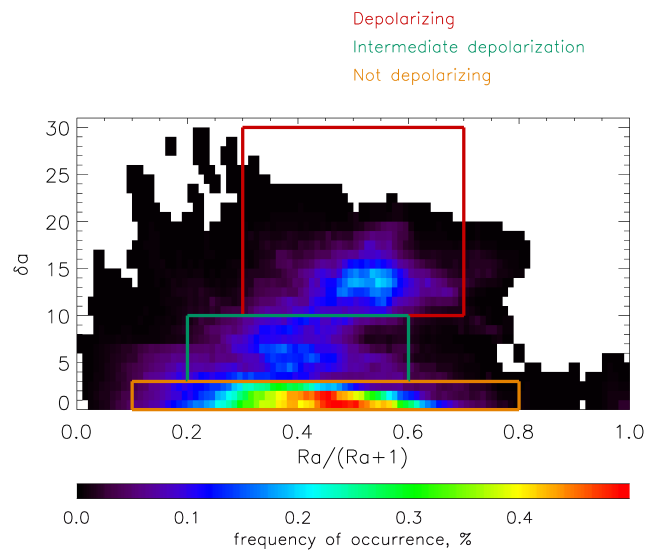
Figure 1. Probability Density Function of aerosol ~~particles~~ particle optical properties over ~~the~~ 15 June – 5 July 2012 as a function of ~~$1-1/R$~~ $Ra/(Ra+1)$ and δ_a parameters. The color code indicates the frequency of occurrence
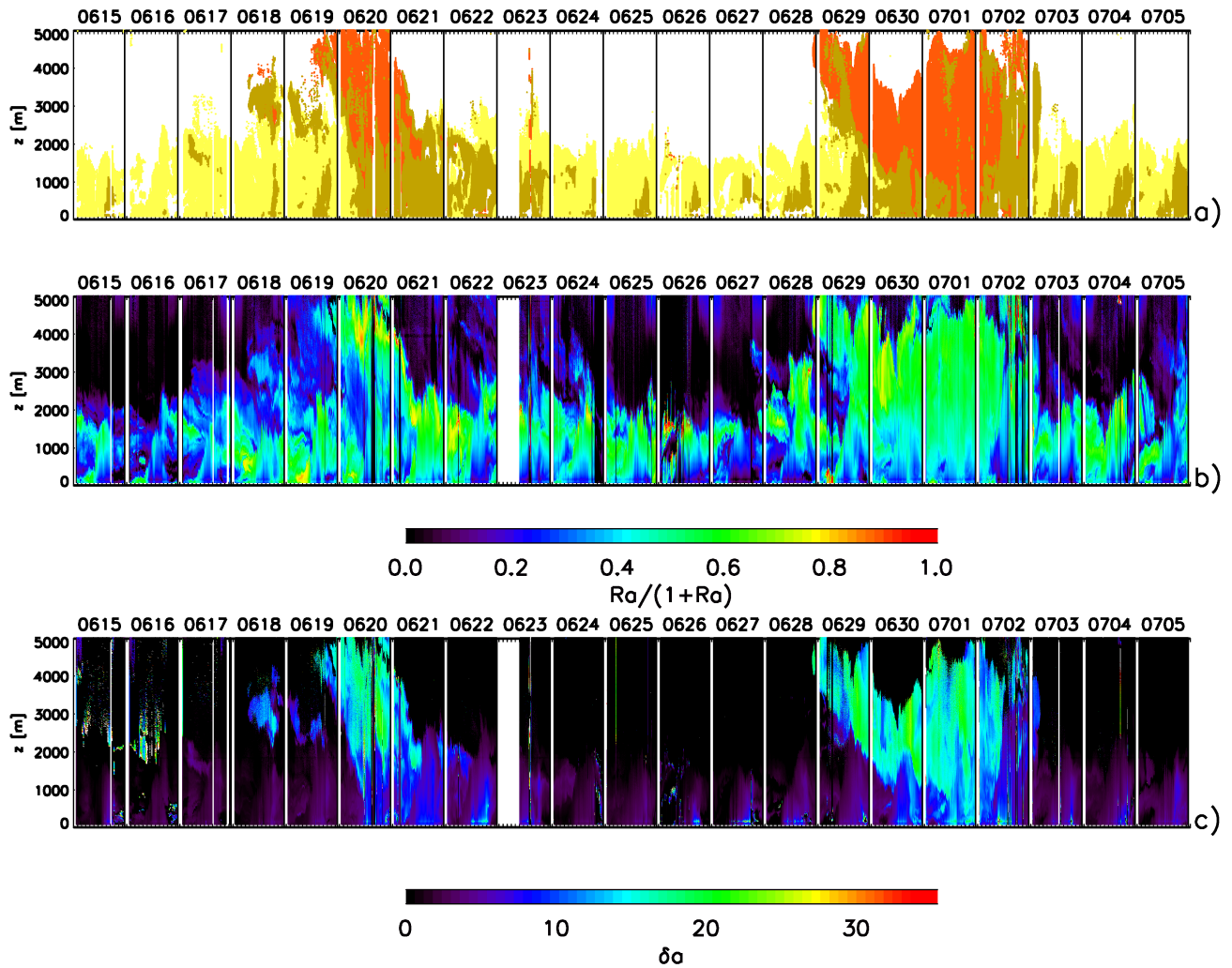
Figure 2. LiDAR observations along the whole campaign. Panel a: vertical profiles of aerosol ~~particles~~ particle types resulting from the classification methodology described by Sec. 3: not depolarizing aerosol (yellow), depolarizing aerosol (orange) and intermediate depolarization aerosol (brown)~~properties~~. Panel b: vertical profiles of ~~1 — 1/R~~ $Ra/(Ra+1)$. Panel c: vertical profiles of δ_a
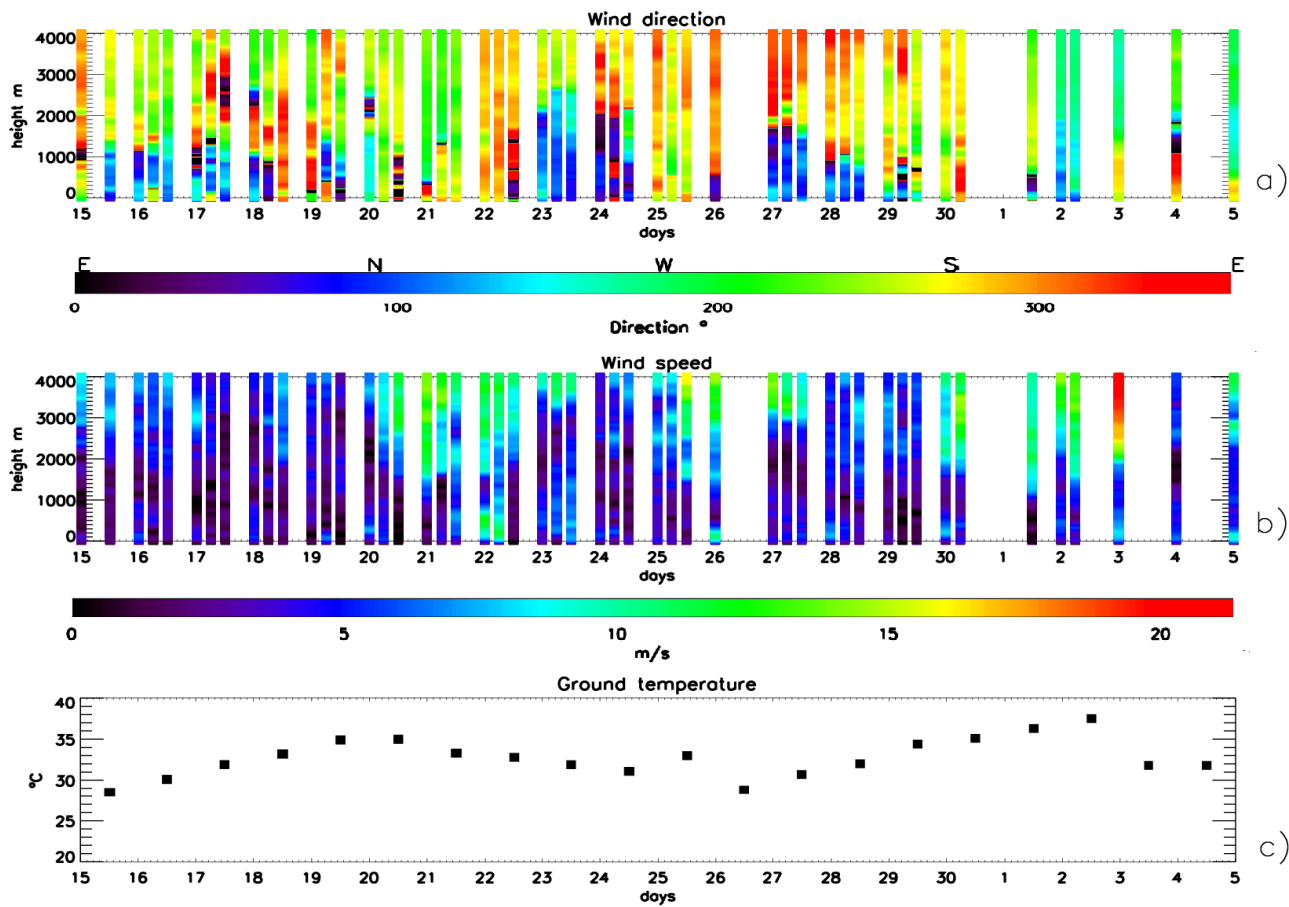
Figure 3. Panel a: wind provenience direction. Panel b: wind speed. Panel c: Ground temperature at 12:00 UTC~~is also reported as red squares, superimposed to the wind speed profiles.~~
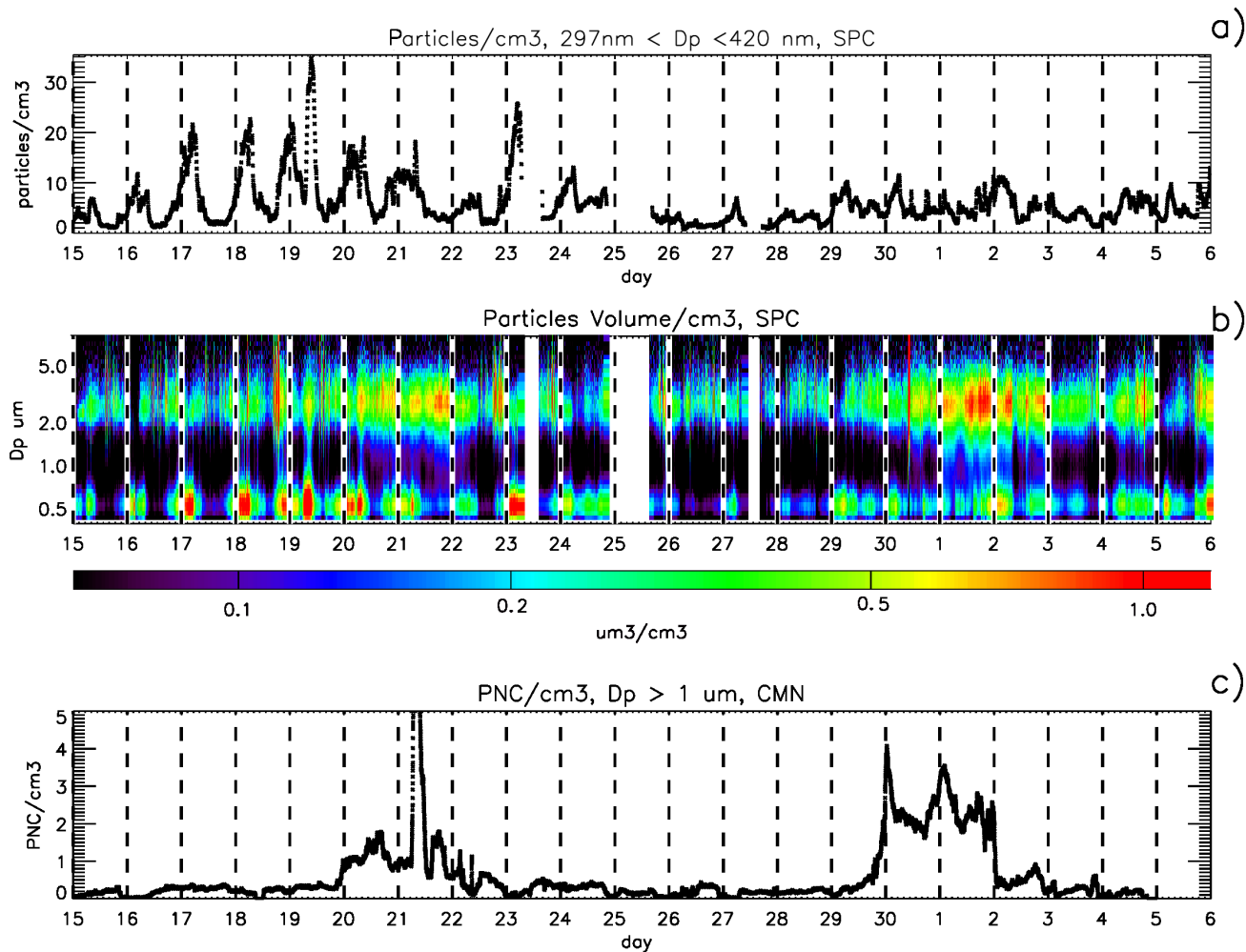
Figure 4. Panel a: APSS particle counts at 297–420 nm of diameter. Panel b: time series of the volume size distribution of aerosol particles asobserved by the APSS. The y-axis indicates the volume-equivalent particle diameters in μm while colours report the corresponding volume concentration. Panel c: time series of coarse ($Dp > 1$μm) particle number concentration observed at CMN
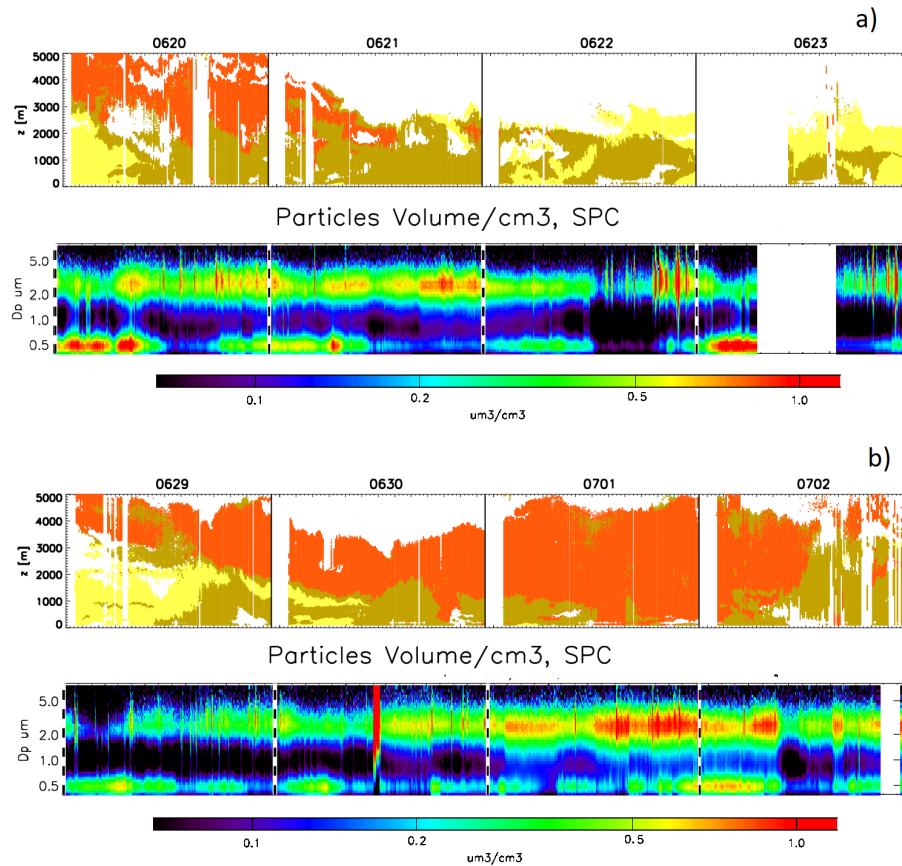
Figure 5. ~~FLEXPART backtrajectories over GFS meteorological input: Panels a and b show the footprint (in~~ Vertical profiles of ~~residence over each bin~~aerosol particle types (upper panel)~~of the trajectories released over SPC at 3000~~, as in Fig~~. Black triangle indicates the point of release~~2~~, black squares mark the position~~ and APSS aerosol time series of the ~~center~~ volume size distribution of ~~mass every 24 hours~~aerosol particles (lower panel), as in Fig~~. The pattern of trajectories released the 20 June at 18:00 UTC are shown on~~ 4, for the ~~left~~ first (panel a) ~~, while pattern released the 29 June at 12:00 UTC on~~ and the ~~right~~ second (panel b) ~~. The simulated~~ dust ~~concentration over the SPC site, derived by the coupling with DREAM, is reported in panel c with a time step of 6 hours. The black line is relative to the particles released at the 1000 – 2000 atmospheric layer and the blue line to the release at 3000 – 4000~~ event
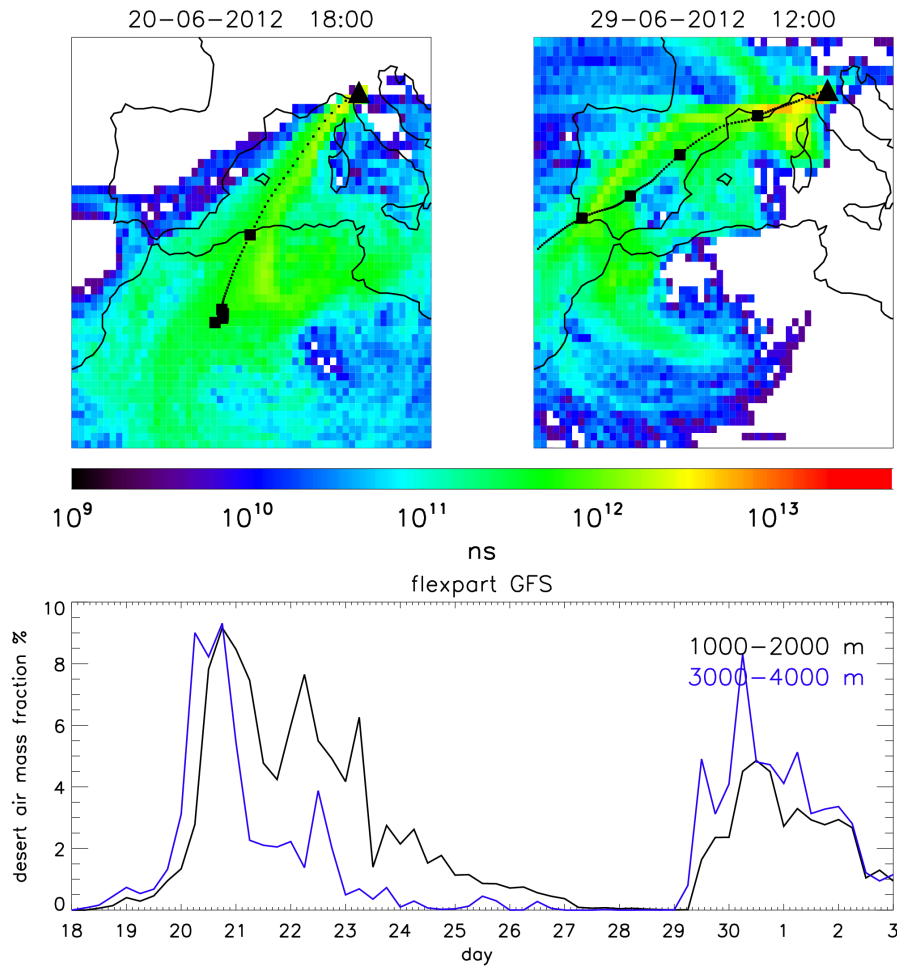
Figure 6. FLEXPART backtrajectories over GFS meteorological input: Panels a and b show the footprint (in ns of residence over each bin) of the trajectories released over SPC at 3000 m. Black triangle indicates the point of release, black squares mark the position of the center of mass every 24 hours. The pattern of trajectories released on 20 June at 18:00 UTC are shown on the left (panel a), while pattern released on 29 June at 12:00 UTC are on the right (panel b). The simulated mass fraction contribution of dust over the SPC site is reported in panel c with a time step of 6 hours. The black line is relative to the particles released at the $1000 - 2000$ m atmospheric layer and the blue line to the release at $3000 - 4000$ m
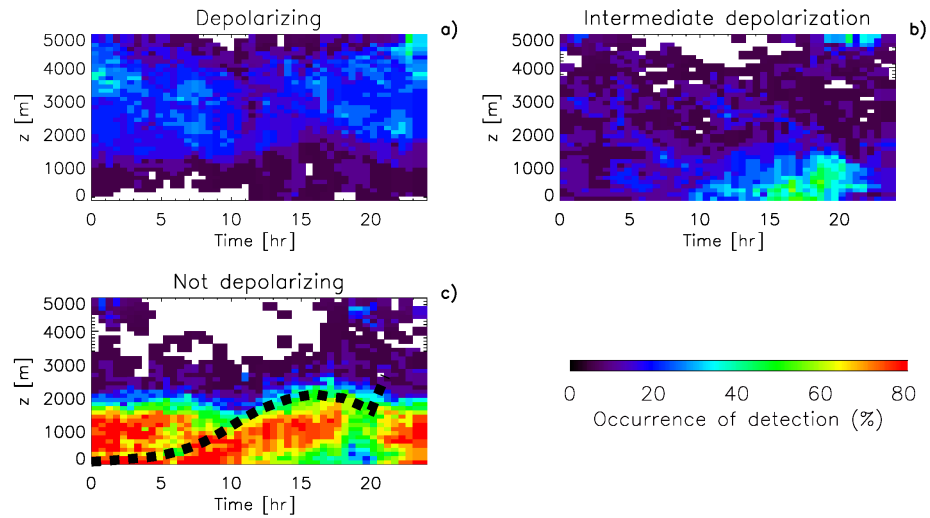
Figure 7. Mean diurnal frequency of the vertical distribution of each aerosol class (computed as the ratio between the number of aerosol class detections and the number of days of measurements): Depolarizing (panel a), Intermediate Depolarizing (panel b) and Non-Depolarizing (panel c). The mean PBL height, derived from LiDAR analysis, is reported in black dashed line over the non-depolarizing particles distribution

~~Mean diurnal frequency of distribution for the three aerosol classes integrated over the four synoptic intervals (00:00–00:06, 06:00–12:00, 12:00–18:00, 18:00–24:00) below 2000 (panel a), above 2000 (panel b) and for the whole atmospheric column 0–5000 (panel c)~~
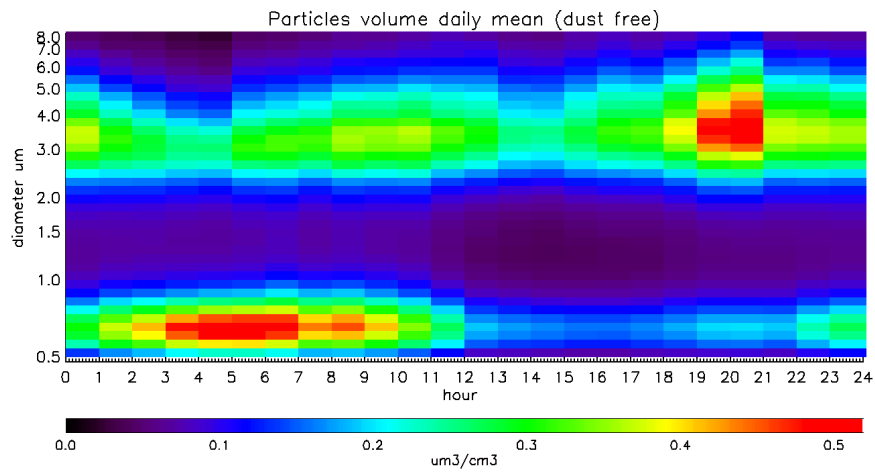
Figure 8. Mean diurnal evolution of aerosol ~~particles~~ particle volume size distribution in dust-free days from the APSS at SPC
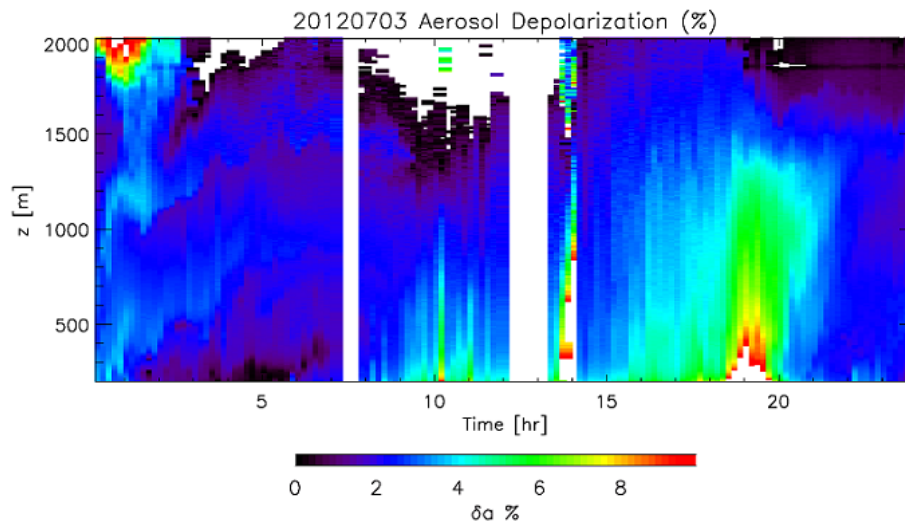
Figure 9. Vertical profiles of LiDAR aerosol ~~particles~~ linear depolarization ratio on ~~the~~ 3 July 2012
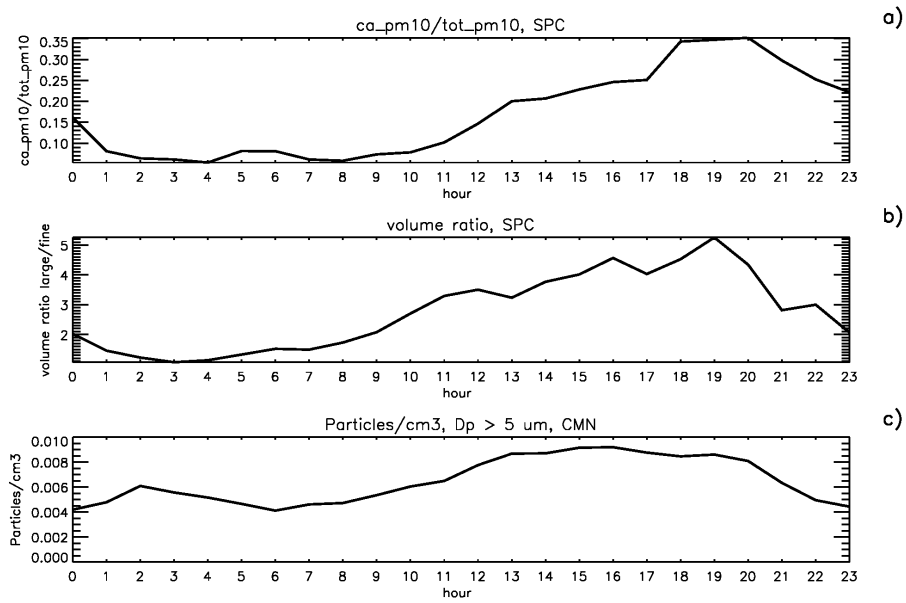
Figure 10. Panel a shows the mean diurnal evolution of the ratio of PM10 concentration of the Calcium ion (Ca2+) over the total PM10 ~~ions~~ ion concentration (Ca2+PM10 /TotalPM10) in SPC. Panel b reports diurnal mean of the ratio of large particles (1 μm < Dp < 5.5 μm) over the fine ones (0.5 μm < Dp < 1 μm) at SPC while panel c shows the diurnal mean of coarse (Dp >5 μm) particles at CMN. Each mean is computed on ~~dust free~~ dust-free days
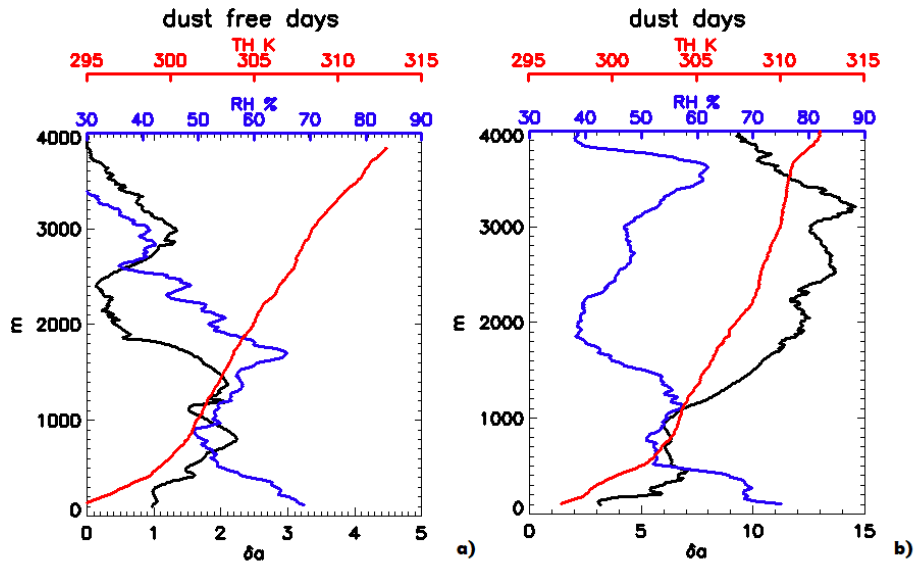
Figure 11. Figure reports the ~~mean~~ vertical profiles of δ_a, RH and ~~the relative humidity from the radiosounding measurements~~ TH for dust-free (panel a) and dust days (panel b) at 05:00 UTC~~overlaid with a different color scale; the timeseries of relative humidity observed at~~. Please notice the ~~ground is reported as a red line~~different horizontal axis for δ_a
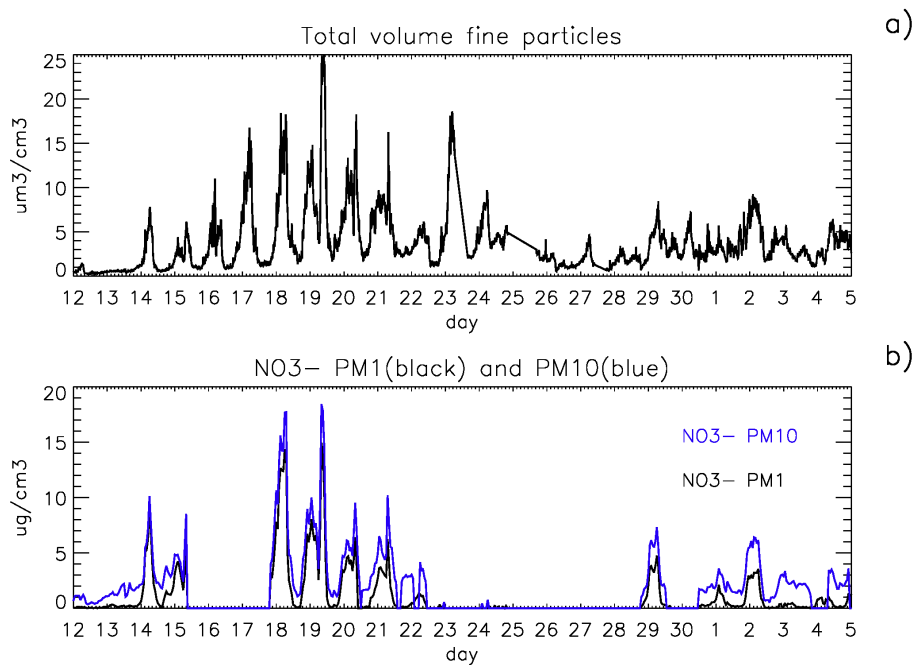
37

Figure 12. APSS fine particles ($Dp < 1$ μm) volume contribution (panel a) compared to nitrates ~~ions~~ ion concentration (NO3−) both in the PM1 (black) and PM10 (blue) channel (panel b). Zero values corresponds to missing observations